8-2006

Sliding mode control of robotics systems actuated by pneumatic muscles.

Liang Yang 1975-
University of Louisville

Recommended Citation

SLIDING MODE CONTROL OF ROBOTICS SYSTEMS
ACTUATED BY PNEUMATIC MUSCLES

By

Liang Yang
B.S., Sichuan University, 1998
M.S., Sichuan University, 2001

A Dissertation
Submitted to the Faculty of the
Graduate School of the University of Louisville
In Partial Fulfillment of the Requirement
for the Degree of

Doctor of Philosophy

Department of Electrical and Computer Engineering
University of Louisville
Louisville, Kentucky

August 2006

SLIDING MODE CONTROL OF ROBOTICS SYSTEMS
ACTUATED BY PNEUMATIC MUSCLES

By

Liang Yang
B.S., Sichuan University, 1998
M.S., Sichuan University, 2001

A Dissertation Approved on

_____

Date

By the following Dissertation Committee:

_____

John H. Lilly, PhD, Dissertation Director

_____

Darrel L. Chenoweth, PhD, Co-Advisor

_____

Joseph D. Cole, PhD

_____

Patricia A. Ralston, PhD

_____

Jacek M. Zurada, PhD

DEDICATION

This dissertation is dedicated to my parents

Mr. Chaoren Yang

and

Ms. Keqing Zhang

who give me great affection and tremendous support.

ACKNOWLEDGEMENTS

ABSTRACT

SLIDING MODE CONTROL OF ROBOTICS SYSTEMS
ACTUATED BY PNEUMATIC MUSCLES

Liang Yang

August 4, 2006

This dissertation is concerned with investigating robust approaches for the control of pneumatic muscle systems. Pneumatic muscle is a novel type of actuator. Besides having a high ratio of power to weight and flexible control of movement, it also exhibits many analogical behaviors to natural skeletal muscle, which makes them the ideal candidate for applications of anthropomorphic robotic systems.

In this dissertation, a new phenomenological model of pneumatic muscle developed in the Human Sensory Feedback Laboratory at Wright Patterson Air Force Base is investigated. The closed loop stability of a one-link planar arm actuated by two pneumatic muscles using linear state feedback is proved.

Robotic systems actuated by pneumatic muscles are time-varying and nonlinear due to load variations and uncertainties of system parameters caused by the effects of heat. Sliding mode control has the advantage that it can provide robust control performance in the presence of model uncertainties. Therefore, it is mainly utilized and further complemented with other control methods in this dissertation to design the appropriate controller to perform the tasks commanded by system operation. First, a sliding mode controller is successfully proposed to track the elbow angle with bounded error in a one-Joint limb system with pneumatic muscles in bicep/tricep configuration. Secondly, fuzzy control, which aims to dynamically adjust the sliding

surface, is used along with sliding mode control. The so-called fuzzy sliding mode control method is applied to control the motion of the end-effector in a two-Joint planar arm actuated by four groups of pneumatic muscles. Through computer simulation, the fuzzy sliding mode control shows very good tracking accuracy superior to nonfuzzy sliding mode control.

Finally, a two-joint planar arm actuated by four groups of pneumatic muscles operated in an assumed industrial environment is presented. Based on the model, an integral sliding mode control scheme is proposed as an ultimate solution to the control of systems actuated by pneumatic muscles. As the theoretical proof and computer simulations show, the integral sliding mode controller, with strong robustness to model uncertainties and external perturbations, is superior for performing the commanded control assignment. Based on the investigation in this dissertation, integral sliding mode control proposed here is a very promising robust control approach to handle systems actuated by pneumatic muscles.

TABLE OF CONTENTS

LIST OF FIGURES

CHAPTER I

INTRODUCTION

1.1   BACKGROUND

Actuators are indispensable for all robots to provide the forces, torques, and mechanical motions to move the joints, limbs, or body. Actuators are generally electric, pneumatic, or hydraulic. Today's mechanical systems have such criteria for actuators as high power density, high power to weight ratio, rapid response, accurate and repeatable control, low cost, cleanliness and high efficiency.

An important area of robotics technology is concerned with the development of manipulators that can replace human beings in the execution of specific tasks. This makes such qualities as light weight, high power, and fast, accurate response even more important for actuators. The pneumatic muscle (PMs) actuator, which possesses many of these advantages, is therefore considered an excellent candidate for robotic applications. However, the inherent nonlinearities, time-varying parameters, and high sensitivity to payload of PMs make it a challenge for the accurate force and position control of manipulators employing these actuators.

This dissertation investigates sliding mode, fuzzy, and integral control techniques for control of robotic systems actuated by PMs. Sliding mode control is a powerful robust control method widely used in variable structure systems, with the feature of strong insensitivities to system uncertainties and nonlinearities. Fuzzy logic is one of the techniques of soft computing. Since it utilizes vagueness in natural language and characterizes system behavior by using human knowledge and

experience, suboptimality and impreciseness can be accommodated, even when providing adequate control. Fuzzy logic uses rules and membership functions to approximate nonlinear functions to any desired degree of precision, which makes it possible to provide quick, simple and sufficiently accurate control for complicated real-world systems. The unique ability of integral control is to bring the controlled variable back to the exact set point following a disturbance. To avoid instability, it is usually combined with another control method. This study will use sliding mode.

1.2 OBJECTIVE

PMs have many characteristics suitable for the application of robot manipulators. The dynamic behavior of the PM has been modeled as a parallel combination of a nonlinear dashpot, a nonlinear spring, and contractile element. Based on this outcome, mathematical models are developed for a one-joint and a two-joint robot manipulator. However, the nonlinear and time varying features of PMs, including variations in load, cause discrepancies between the actual plant and the ideal mathematical model developed for controller design.

Sliding mode control (SMC) has the ability to tackle the parametric and modeling uncertainties of nonlinear systems. The robustness to system uncertainties makes it an ideal candidate for the control of systems containing PMs. In this research, a sliding mode controller is designed to force the end effector of a two-joint planar manipulator to track a spatial reference trajectory. This proposed sliding mode controller makes the planar manipulator relatively insensitive to parameter fluctuations.

"Chattering" is a natural byproduct of the sliding mode approach. It is caused by the control switches when the system state crosses a sliding surface. Chattering is undesirable because it increases control effort and excites

2

high-frequency modes of the system. To reduce chattering, a boundary layer is usually introduced around the sliding surface. However, the introduction of this boundary layer causes increased tracking error. To decrease tracking error while reducing chattering, the control bandwidth in the sliding surface is adjusted according to the variance of tracking error.

Fuzzy logic, using natural language to describe system behavior, provides a simple and effective way to tune control bandwidth. Accordingly, a so-called fuzzy sliding mode controller (FSMC) is designed for the two-joint robot manipulator. The performance of the planar manipulator controlled with FSMC is shown to be superior to that using standard SMC.

Since the robot manipulator is a physical system in real life, external perturbations may always be assumed to exist. This requires an external noise component added to the previous model. Based on this assumption, integral control is applied for disturbance rejection. An integral sliding mode control approach (ISMC) is then used to combine the disturbance rejection benefits of integral control with the robustness properties of SMC. Simulations show that ISMC has strong robustness to system parameter uncertainties and external disturbance throughout the process of control, giving excellent tracking accuracy with no chattering. The conclusion can be drawn that the proposed ISMC is a promising candidate for the control of robot manipulators actuated by PMs.

1.3 Dissertation Outline

Chapter 2 reviews the literature regarding the development of pneumatic actuators and pneumatic muscle, robotic manipulators and sliding mode control and its application. References on control applications to robotics of PMs, fuzzy logic,

and integral control are included as well. Chapter 3 gives the background knowledge of pneumatic muscle actuator and robotics technology. Chapter 4 overviews the relevant control methods used in this paper, which includes sliding mode control, fuzzy control and integral control. Chapter 5 introduces the PM mathematical model used in this research. The stability of a PM under closed-loop state feedback control is analyzed. In addition, heating effects of the PM is addressed.

Chapter 6 discusses a two-link, single-joint robot manipulator actuated by antagonistic pneumatic muscle actuator groups. Based on the derived model, a sliding mode controller is proposed to produce accurate tracking of the elbow angle. Simulations verify good tracking performance of the system under sliding mode control. The chattering phenomenon is almost eliminated by introducing a boundary layer around the sliding surface.

Chapter 7 presents a three-link, two-joint robot manipulator actuated by four PM groups. To improve tracking accuracy while maintaining robustness, the control bandwidth is tuned by using fuzzy logic, which results in two time-varying sliding surfaces. This is the so-called fuzzy sliding mode approach. Simulation results verify that the proposed fuzzy sliding mode controller has better tracking performance than nonfuzzy sliding mode controller for PM-actuated systems.

Chapter 8 further discusses the improvement of the two-joint robot manipulator described in Chapter 7. The model is now considered to be corrupted with an external perturbation. An integral sliding surface is formulated for disturbance rejection. Simulations verify that the proposed integral sliding mode control method not only has strong robustness to system uncertainties and external perturbations but also makes tracking more accurate than traditional sliding mode

4

control while chattering is avoided as well.

Chapter 9 draws the conclusions based on the findings of previous chapters, and the main contributions of this dissertation are addressed.

CHAPTER II

LITERATURE REVIEW

Research in pneumatic muscle actuators and their applications has been undertaken in many places.   Comer claimed a pneumatic muscle analog as his patent [65].   Being used in opposition, the artificial muscles synergistically assist each other and are easily controlled by the associated simple low-cost control systems.   Krauter invented a bistep terminator for pneumatic muscle, by which pneumatic muscle can withstand high axial tensile forces and high internal fluid pressures [66].

The Intelligent Robotics Lab at Vanderbilt has developed a mobile robot powered by PMs, named ROBIN (for ROBotic INspector), which is used for inspection of many types of structures.   ROBIN's advantages include light weight and high mobility, being able to walk on horizontal or vertical surfaces and step over obstacles.   Another PM system, the "Intelligent Soft Arm," was also developed at Vanderbilt to provide actuation for an intelligent robotic aid system for the service sector such as hospitals and home.   The system is named ISAC, for Intelligent Soft Arm Control.   The main application of ISAC is to provide the sick and physically challenged person with means to live independently. [2, 3].

Work related to the physical properties and applications of PMs was studied at the University of Salford, U.K. [4, 5, 6, 7].   They found the bandwidth limit of PMs could be improved by reducing the dead volume within the muscle structure and ensuring effective air flow rates.   They also have developed new models and pneumatic muscle actuators with extremely high power/weight ratio and applied them

to bipedal and humanoid robots, quadruped robots etc.

The BioRobotics lab at the University of Washington has several research projects that utilize PMs [9, 10, 11]. The powered prosthetics project addresses the problem of amputee walking via a PM-powered prosthesis. The lab is also concerned with issues such as finite-element modeling and fatigue properties of PMs.

In addition to the work mentioned above, there have been many other researchers investigating some aspect of PM control. In [8], a classic nonlinear estimator algorithm was applied to nonlinear parametric identification of a McKibben artificial pneumatic muscle. In [12], a pneumatic muscle-driven hand therapy device was developed for volitional activation of joint movement while providing related information about motion and muscle activity.

Much research regarding robot manipulators actuated by PMs has been carried out in recent years. Noritsugu *et al*. in Okayama University, Japan, investigated PM actuation and control of rehabilitation robots [14, 15, 16]. They developed a pneumatic therapy robot, which is able to implement various motion modes by an impedance control strategy. A pneumatic haptic interface was designed to realize information transfer as well. In addition, they improve the control performance of a PM actuator with a variable damper using electrorheological fluid.

Similarly, a Multi-module Deployable Manipulator System (MDMS) was developed at the University of British Columbia [17]. In [18], a wheelchair-mounted pneumatic robot arm for disabled children was designed, consisting of a four-bar transmission mechanism driven by two Flexator actuators, which are similar to PMs. In [19], a cable-driven manipulator using pneumatic artificial muscle actuators was developed to control the orientation and insertion depth of an endoscope during abdominal surgery. In [20], a retrieval rig was constructed by utilizing a

7

combination of a traditional human-manipulated pole and pneumatic muscle actuators.

Because the parameters of robot manipulators are dependent on the manipulator structure and the payload, it is very difficult to obtain exact values for them. Therefore the investigations upon the effective control of robot manipulators have been carried on. In [67], on the basis of information of a third homogeneous transformation matrix, a manipulator can be controlled at a desired position and attitude in the absolute space irrespective of a condition of traveling on standstill of the moving body. In [69], a calculation corresponding to a special algorithm of inverse kinematics is utilized the Jacobi Matrix in the control of a manipulator, which can be used in interactive path guidance of a manipulator.

Furthermore, these parameters along with those of pneumatic muscle actuators themselves are nonlinear and time-varying. Uncertainties, hence, always exist. Sliding mode control (SMC) has long been used for dealing with nonlinear uncertain systems, and many applications of SMC in conjunction with PM actuation can be found. Gamble patents a control method and apparatus for a moveable control member [68]. The apparatus incorporates a sliding mode control system operable to maintain the state point of the moveable member on a predetermined non-linear hyperplane. Yoneda proposes a way for maintaining a controlled system on a switching hyperplane regardless of the magnitude of disturbance [70]. In [22], a new position control algorithm based on sliding mode control, has been developed for a pneumatic cylinder as an actuator for robot manipulators. In [23], the advantages and disadvantages of sliding mode control have been studied and compared with those of two other robust control methods. In [24], for the trajectory control of robot manipulators, a sliding-mode control algorithm is used to estimate the unknown

parameter bounds. In [25], a sliding mode control algorithm is designed for a benchmark direct-drive robot. In [26], a sliding mode controller is developed for a two-link rigid robotic manipulator with uncertain modeling. In [27], a decoupled sliding mode control algorithm is constructed for the position control of a PUMA 560 robot arm. In [28], for stabilization of robot manipulator systems with parameter perturbations, a new continuous sliding mode controller is designed. In [29], a sliding mode controller based on motor angular speed control has been developed for a robot manipulator with payload variation.

In addition to standard SMC, this research also considers SMC combined with fuzzy logic as a possible improvement on the control of robotic systems actuated by PMs. Since fuzzy logic collects human knowledge and expertise, it is an effective solution to handle control problems with unknown or poorly known models. It can not only serve as an independent powerful control approach but also be a useful complementary tool for sliding mode control of robotics systems.

Many robotics control applications that exploit fuzzy logic have been investigated. In [30], a fuzzy logic controller is proposed for a robot manipulator with uncertainties. In [31], a fuzzy control system was show to be effective for motion tracking control of robot manipulators. In [32], in order to guarantee both global stability and accurate performance, a fuzzy controller was designed for robust control of robot manipulators. In [33], to compensate for unmodeled dynamics and reduce chattering, a sliding mode controller complemented with a fuzzy logic scheme is proposed for the trajectory control of a robot manipulator. In [34], a sliding mode controller is introduced to the end effector position control of a manipulator. A fuzzy weighting factor is considered to regulate control input for better position control and vibration reduction.

For the elimination of tracking error, integral control is a very useful supplement to many other control methods. Combined with sliding mode control, it shows good effectiveness in quite a few robotics applications. At Universiti Tcknologi Malaysia, Ahmed *et al*. designed a series of sliding mode controllers, which take advantage of proportional-integral control to track the motion of robot manipulators [35, 36, 37]. In [38], the stability of a closed-loop system controlled with an integral sliding mode strategy is analyzed using Lyapunov stability theory. In [39], a class of integral sliding mode designs is addressed, having potential to be applied in a wide area. In [40], a tracking motion control of a helicopter is studied to show that the proposed controller is able to guarantee system stability with robustness to uncertainties.

CHAPTER III

INTRODUCTION TO PNEUMATIC MUSCLE ACTUATORS AND ROBOTICS

3.1 INTRODUCTION TO PNEUMATIC MUSCLE ACTUATORS

Pneumatic Actuators

Actuators are essential components in any control system, converting energy into mechanical form.   There are three main classes of actuators depending on the source of energy available: electric, pneumatic, and hydraulic.   The advantages and disadvantages of these types of actuators are listed in Table 1.

Table 1   Characteristics of Major Actuators

Actuators	Electric	Pneumatic	Hydraulic
Advantages	1. quiet operation 2. cheapness 3. accuracy	1. high power to weight ratio 2. high bandwidth 3. cheapness 4. cleanness, safety of operation 5. compactness	1. high power capability 2. high accuracy 3. self-cooling
Disadvantages	1. low power to weight ratio 2. possible sparking	1. difficult to control accurately 2. compliance 3. time delay	1. highly nonlinear 2. less reliable 3. dangerous if fails 4. expensive

Typically, electrical actuators are better suited to high speed, low load

applications, while hydraulic actuators do better at low speed and high load applications. Pneumatic actuators refer to the devices in which compressed air is used to control and operate equipment. Pneumatic actuators are like hydraulic actuators except that they are not generally used for high payload.

Presently, more importance is placed on light weight, high power, and fast, accurate response in the field of robotics technology. Traditionally, electrical and hydraulic actuators have been selected as the preferred drive mechanism, but these have well documented limitations, especially where compactness and high power/weight are needed for applications such as dexterous manipulation and multi degree of freedom arms. In addition, both electrical and hydraulic actuator have such rigid behavior that they can only be made to act in a compliant (i.e. soft) manner at the cost of more complicated physical structures and control strategies.

Therefore, pneumatic actuators have become an important source of motive power for robot manipulators. Nevertheless, robotic systems require accurate control of velocity or position of joints and links. However, as mentioned above, the uncertain nature of pneumatic actuators render them unable to give satisfactory actuation for robotic applications.

Pneumatic Muscle

The McKibben Artificial Muscle shown in Figure 1 [9, 10, 11] later built by Washington Biorobotics Lab, first appeared in the 1950s as part of an artificial limb system. This actuator was later called the pneumatic muscle (PMs) because of its similarity to human muscle. Some major advantages of PMs are spring-like behavior, extremely light weight and physical flexibility. In addition, PMs exhibit many analogical behaviors to natural skeletal muscle, which makes them ideal for applications of anthropomorphic robotic systems.
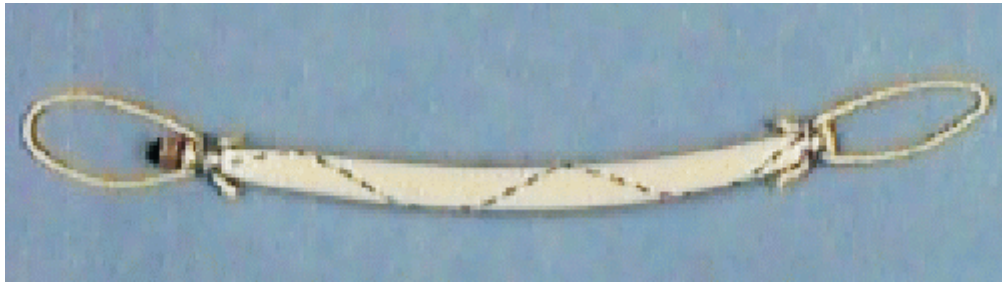
Figure 1 - McKibben Artificial Muscle.
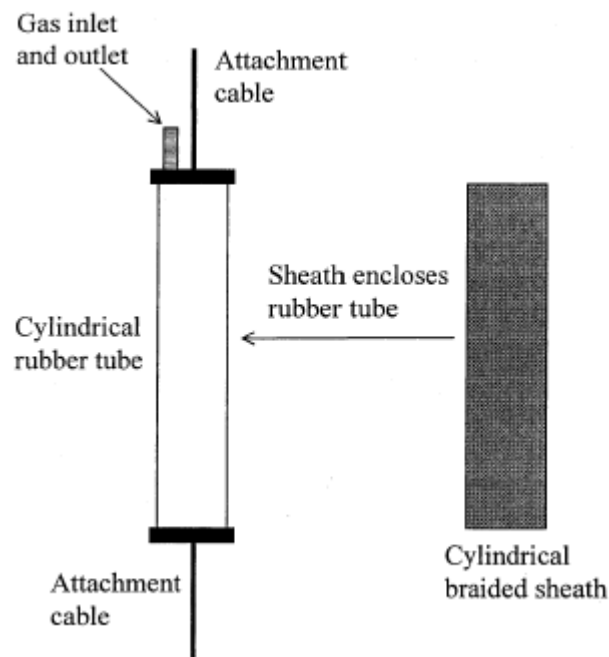
Figure 2 - Construction of PMs

As Figure 2 shows [48], a PM is composed of a flexible reinforced thin inner rubber tube covered by a double helix cordage braid which transforms a radial force into an axial contraction force. The muscle has two ends; one is used for supplying air pressure inside the rubber tube while the second end is used for transferring the muscle force to an external object. When pressure increases in the rubber tube, a contraction axial force is produced, with the length of rubber decreasing and radius increasing. The force and motion generated thus are linear and unidirectional. The

13

PM works similarly to human or animal muscle, in that a force or moment is only created through the action of a contraction. When the tube is inflated, it widens and due to the braided sheath, the entire assembly shortens. The force exerted when the muscle shortens is quite large in proportion to the muscle weight.

PMs have many exciting characteristics suitable for robotic applications. In addition to exceptionally high power to weight and force to volume ratios, the actual achievable displacement, or "stroke" is dependent on the construction and loading but is typically 30 percent of the dilated length. The pneumatic muscle is highly flexible, soft in contact and has excellent safety potential, which is comparable with the contraction achievable in natural muscle. Energy efficiency in conversion of pneumatic to mechanical energy is up to 50 percent and the contractile force for a given cross-sectional area of actuator can be over $300N/cm^2$ compared with $20-40N/cm^2$ for natural human muscle. Finally, the actuators can operate safely in liquid, gaseous, or explosive environments.

In spite of PMs' attractive features, the difficulty and accuracy of force and position control limits their widespread applications for robotic technology. In addition, nonlinearities and time-varying system parameters caused by compliance and weave angle dynamics, which are inherent to PMs in the process of controlling force and position, presents a challenging problem for modeling and control.

3.2 BASICS OF ROBOT MANIPULATORS

Introduction to Robotics

Robotics has undergone an outstanding development over the past few decades due to the increasing demand for not only higher levels of productivity and quality regarding industrial activities but also for more advanced automation systems

by which tedious and potentially harmful tasks can be performed. Robotics is an attractive interdisciplinary field of study involving materials, manufacturing, physics, electronics, statics and dynamics, control theory, etc. The knowledge of materials and manufacturing is helpful for robot construction. Physics and electronics are utilized to design sensors and interfaces. Statics and dynamics are used to describe the behavior and control theory provides methodologies for designing algorithms to implement desired motions.
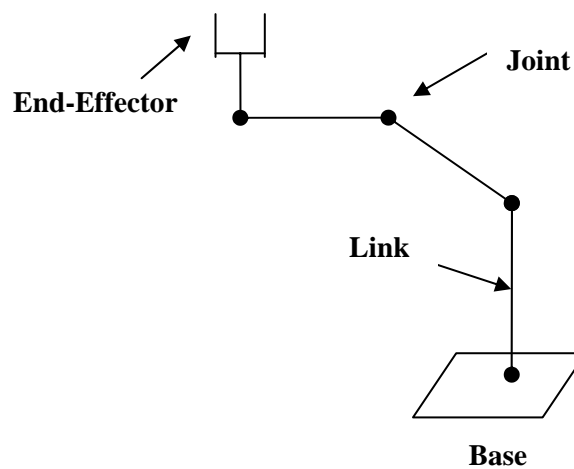
Figure 3 - Simplified structure of robot manipulator

The Robotic Industries Association defines an industrial robot i.e. robot manipulator, as follows: An industrial robot is a reprogrammable, multifunctional manipulator designed to move materials, parts, tools, or specialized devices through variable programmed motions for the performance of a variety of tasks. A robot manipulator can be modeled as a chain of rigid links, which are interconnected to each other by joints as illustrated in Figure 3 [58]. Generally, one end of the chain is fixed to a base and the other end, called the end-effector, is free to move.

It is crucial to be able to position the end effector in the right place at the right instances in the process of performing a task. In other words, to control a robot manipulator is to make its end-effector follow a preplanned desired path to handle

objects in the workspace. For such a path-planning problem, many issues need to be addressed, such as keeping the planned path within the voltage and torque limitations of the actuators and avoiding obstacles.

In order to design the motion of the end-effector, the relationship between it and the joint angles must be formulated. Given the joint variables of a robot manipulator, to determine the position of the end-effector regarding a coordinate frame attached to the robot base is the so-called direct kinematics problem. The solution to the direct kinematics problem is quite useful since it gives an explicit relationship that shows the dependence of the end-effector position on the joint variables. A systematic procedure called the Denavit-Hartenberg algorithm is the general method to solve the direct kinematics problem.

Conversely, to determine the joint variables given a desired position of the end-effector is called the inverse kinematics problem. The latter is important because robot manipulation tasks are usually formulated in terms of the desired end-effector paths and positions. The inverse kinematics problem is also more difficult due to the fact that a systematic closed-form solution is generally not available. In addition, the closed-form solutions may not be unique; that is, different joint variables may yield the same position value for the end-effector, and the manipulator controller has to be able to choose one according to some criteria.

Inverse Kinematics of Planar Arm

A robot manipulator is considered solvable if the joint variables can be determined by an algorithm that is able to determine all the sets of joint variables corresponding to a given end-effector position.
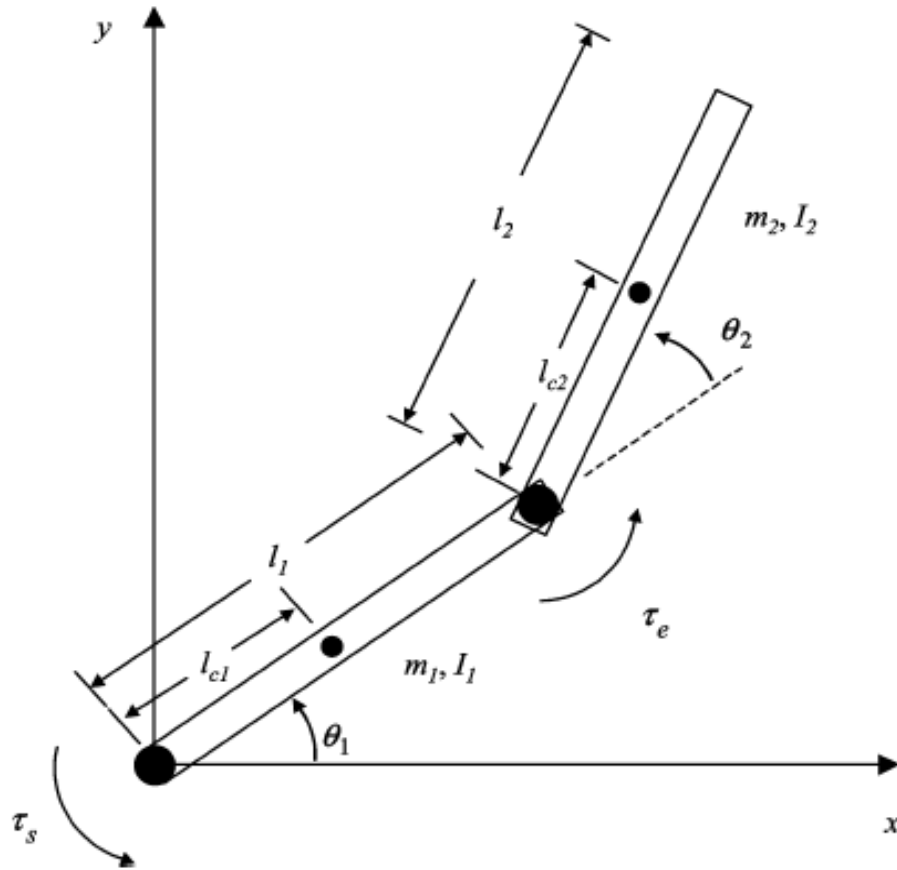
Figure 4 - Configuration of planar arm

The two-link planar arm is one typical kind of robot manipulator, the design principle and analysis procedure of which are very helpful for understanding more complicated manipulators. The solution to the planar arm direct and inverse kinematics is well known [58]. The configuration of a two-joint planar arm is depicted in Figure 4 [58]. In Figure 4, l_i denotes the length of link i, l_{ci} denotes the distance from the previous joint to the center of mass of link i (center of mass is denoted by a dot), and I_i denotes the moment of inertia of link i about an axis coming out of the page, passing through the center of mass of link i.

The dynamics of this system is described by

$$D(\theta)\ddot{\theta} + C(\theta,\dot{\theta})\dot{\theta} + f(\theta) = \tau \qquad (3.1)$$

17

where $\theta = [\theta_1, \theta_2]^T$ is the vector of joint angles and $\tau = [\tau_s, \tau_e]^T$ is the vector of input torques. The nonsingular inertia matrix $D(\theta)$ is

$$D(\theta) = \begin{bmatrix} d_{11} & d_{12} \\ d_{21} & d_{22} \end{bmatrix} \tag{3.2}$$

where

$$d_{11} = m_1 l_{c1}^2 + m_2 (l_1^2 + l_{c2}^2 + 2 l_1 l_{c2} \cos\theta_2) + I_1 + I_2 \tag{3.3a}$$

$$d_{12} = d_{21} = m_2 (l_{c2}^2 + l_1 l_{c2} \cos\theta_2) \tag{3.3b}$$

$$d_{22} = m_2 l_{c2}^2 + I_2 \tag{3.3c}$$

and $I_i = m_i l_{ci}^2, i = 1, 2.$ The matrix $C(\theta, \dot{\theta})$ is given as:

$$C(\theta, \dot{\theta}) = \begin{bmatrix} h\dot{\theta}_2 & h\dot{\theta}_2 + h\dot{\theta}_1 \\ -h\dot{\theta}_1 & 0 \end{bmatrix} \tag{3.4}$$

with $h = -m_2 l_1 l_{c2} \sin\theta_2.$ The vector $f(\theta)$ in (3.1) is given by $f(\theta) = [f_1, f_2]^T$ where

$$f_1 = (m_1 l_{c1} + m_2 l_1) g \cos\theta_1 + m_2 l_{c2} g \cos(\theta_1 + \theta_2) \tag{3.5a}$$

$$f_2 = m_2 l_{c2} g \cos(\theta_1 + \theta_2) \tag{3.5b}$$

and g is the acceleration of gravity.

If desired end-effector spatial trajectories $x_d(t), y_d(t)$ are given, then from the inverse kinematics of the planar arm, it is well known [13] that these spatial path requirements are equivalent to required joint trajectories of

$$\theta_2^*(t) = \cos^{-1} \frac{(x_d^2 + y_d^2 - l_1^2 - l_2^2)}{2 l_1 l_2} \tag{3.6a}$$

18

$$\theta_1^*(t) = \tan^{-1}\left(\frac{y_d}{x_d}\right) - \tan^{-1}\left[\frac{(l_2 \sin\theta_2^*)}{(l_1 + l_2 \cos\theta_2^*)}\right] \qquad (3.6b)$$

In a robot system, there are many uncertainties such as changing parameters i.e. inertia and payload variations. Traditional linear controllers have many difficulties in dealing with these uncertainties. It is even more challenging to control robot manipulators if they are actuated by PMs because the actuators themselves have nonlinear and time-varying characteristics. Therefore, two control approaches known to be robust to model uncertainties, sliding mode control and fuzzy control, are applied for control of robotic manipulators actuated by PMs.

CHAPTER 4

OVERVIEW OF CONTROL METHODS USED IN THIS RESEARCH

4.1   SLIDING MODE CONTROL

Introduction

Systems with structural uncertainties or very complicated structures are difficult to control. Modeling of the uncertainties or handling the deterministic complexity are typical problems encountered frequently in the field of systems and control engineering. It is well known that the most precise detailed model leads to more complicated structure hence the cost increases dramatically. On the other hand, since stability and robustness are of crucial importance in control engineering practice, implementation oriented control engineers endeavor to make a control design insensitive to environmental disturbances and structural uncertainties.

One way of dealing with uncertainties without the use of complicated models is to introduce robust control theory into the system control design. The typical structure of a robust controller is composed of both a nominal part, similar to a feedback control law, and additional terms for dealing with model uncertainty. Sliding mode control is one important type of robust control. Model imprecision may come from actual uncertainty about the plant or from a purposeful simplification of the system's dynamics. Modeling inaccuracies can cause strong adverse effects on the control design of nonlinear systems. For the class of systems to which it applies, sliding mode controller design provides a systematic approach to the problem of

maintaining stability and consistent performance in the face of modeling imprecision.

The idea of sliding mode control is to achieve some desired control performance described by a predefined surface called the sliding surface. The sliding surface is a surface in the state space containing the desired operating point. In general, two phases are involved during the operation of sliding mode control. In the first phase, or reaching phase, the system states are brought from their initial conditions to the sliding surface. In the second phase, or sliding phase, the states move along the sliding surface to the desired operating point, thus making the system obtain the desired performance.

Sliding mode control is essentially a high-speed switched feedback control. The switching control law drives the state trajectory of the nonlinear system onto the sliding surface in the state space and maintains the state trajectory on this surface for all subsequent time. The feedback switches based on a rule determined by the state variables at each instant. Specifically, when the state trajectory is on one side of the surface, feedback path has one gain and a different gain if the trajectory crosses the surface. Obviously, the sliding surface defines the rule for proper switching.

Sliding Mode Control Design

For stability purposes, the most important task is to design a sliding mode control law that will drive the system state to the sliding surface and maintain it on the surface once it has been reached. A Lyapunov approach is generally used to regulate the motion of the system trajectory to the sliding surface. The sliding mode control law chooses the gain for each switching so that the derivative of a Lyapunov function is negative definite, which guarantees motion of the system trajectory to the surface. Once the sliding surface is properly designed, the resulting controller forces the system trajectory to approach the sliding surface such that the system state variable is

driven to and maintained on the sliding surface.

Consider the following second order single-input nonlinear dynamical system [21]:

$$\ddot{x} = f(x, \dot{x}) + bu \tag{4.1}$$

where x is the scalar system state and u is the scalar control input. Suppose the dynamics f is not exactly known but is estimated as $\hat{f}$. Let $F(x, \dot{x})$ be a positive function such that

$$\left| \hat{f} - f \right| \le F \tag{4.2}$$

The nonunity control gain b is unknown but of known bounds $0 < b_{min} \le b \le b_{max}$. Choose the estimation $\hat{b}$ of gain as the geometric mean of the above bounds:

$$\hat{b} = \sqrt{b_{min} b_{max}} \tag{4.3a}$$

$$\beta = \sqrt{(b_{max} / b_{min})} \tag{4.3b}$$

$$\beta^{-1} \le b\hat{b}^{-1} \le \beta \tag{4.3c}$$

Let $x_d(t)$ be the desired state trajectory, and define tracking error $\tilde{x} = x - x_d$. Define the sliding surface $s(t)$ as

$$s = \dot{\tilde{x}} + \lambda \tilde{x} \tag{4.4}$$

To eliminate chattering, consider a boundary layer enclosing the switching surface $B(t) = \{x, |s(x;t)| \le \Phi\}, \Phi > 0$ and define a function

$$k = \beta(F + \eta) + (\beta - 1)|\hat{u}| \tag{4.5}$$

where $\hat{u} = (-\hat{f} + \ddot{x}_d - \lambda\dot{\tilde{x}})$ and η is a positive constant. The sliding mode control law is then proposed [21]:

$$u = (\hat{u} - k\text{sat}(s/\Phi))\hat{b}^{-1} \qquad (4.6)$$

where Φ is the boundary layer thickness and sat is the saturation function, defined as:

$$\text{sat}(y) = \begin{cases} y, & |y| \le 1 \\ \text{sgn}(y), & \text{otherwise} \end{cases} \qquad (4.7)$$

Then the following basic result is acquired concerning the tracking performance of the sliding mode controller outlined above.

Theorem 1: The sliding mode control law (4.6) applied to the uncertain nonlinear system (4.1) results in

$$\lim_{t_0 \to \infty} \sup_{t \ge t_0} |x(t) - x_d(t)| \le \frac{\Phi}{\lambda} \qquad (4.8)$$

Proof: Differentiating (4.4), we obtain

$$\dot{s} = bu + f - \ddot{x}_d + \lambda\dot{\tilde{x}} \qquad (4.9)$$

Substituting (4.6) into (4.9) gives

$$\dot{s} = f - b\hat{b}^{-1}\hat{f} + (1 - \hat{b}b^{-1})(-\ddot{x}_d + \lambda\dot{\tilde{x}}) - b\hat{b}^{-1}k\text{sat}(s/\Phi) \qquad (4.10)$$

Noticing that $\beta^{-1} \le b\hat{b}^{-1} \le \beta$ and $1 \le \beta$, we have

$$k \ge \hat{b}b^{-1}F + \eta\hat{b}b^{-1} + (\hat{b}b^{-1} - 1)\left|\hat{f} - \ddot{x}_d + \lambda\dot{\tilde{x}}\right| \tag{4.11}$$

Since $f = \hat{f} + (f - \hat{f})$ where $\left|f - \hat{f}\right| \le F$, this gives

$$k \ge \left|\hat{b}b^{-1}f - \hat{f} + (\hat{b}b^{-1} - 1)(-\ddot{x}_d + \lambda\dot{\tilde{x}})\right| + \eta\hat{b}b^{-1} \tag{4.12}$$

In particular,

$$k = \left|\hat{b}b^{-1}f - \hat{f} + (\hat{b}b^{-1} - 1)(-\ddot{x}_d + \lambda\dot{\tilde{x}})\right| + \eta\hat{b}b^{-1} \tag{4.13}$$

Substituting (4.13) into (4.10), we have

$$\dot{s} = f - b\hat{b}^{-1}\hat{f} + (1 - b\hat{b}^{-1})(-\ddot{x}_d + \lambda\dot{\tilde{x}}) - \left(\left|f - b\hat{b}^{-1}\hat{f} + (1 - b\hat{b}^{-1})(-\ddot{x}_d + \lambda\dot{\tilde{x}})\right| + \eta\right)\mathrm{sat}(s/\Phi)$$

$$\tag{4.14}$$

First, consider the case that the trajectory $x(t)$ is outside $B(t)$, then (4.14) becomes

$$\dot{s} = f - b\hat{b}^{-1}\hat{f} + (1 - b\hat{b}^{-1})(-\ddot{x}_d + \lambda\dot{\tilde{x}}) - \left(\left|f - b\hat{b}^{-1}\hat{f} + (1 - b\hat{b}^{-1})(-\ddot{x}_d + \lambda\dot{\tilde{x}})\right| + \eta\right)\mathrm{sgn}(s)$$

$$\tag{4.15}$$

which is then rewritten as:

$$\dot{s} = w - (|w| + \eta)\mathrm{sgn}(s) \tag{4.16}$$

where $w = f - b\hat{b}^{-1}\hat{f} + (1 - \hat{b}b^{-1})(-\ddot{x}_d + \lambda\dot{\tilde{x}})$. In this case

$$
\begin{aligned}
\frac{1}{2}\frac{d}{dt}(s^2) &= \dot{s}s \\
&= (w - (|w| + \eta)\operatorname{sgn}(s))s \\
&= ws - (|w| + \eta)\operatorname{sgn}(s)s \\
&\leq |ws| - (|w| + \eta)|s| \\
&= -\eta|s| < 0
\end{aligned}
\tag{4.17}
$$

i.e. the trajectory approaches the boundary layer.

Secondly, consider the case that s is inside $B(t)$. In this case (4.14) becomes:

$$
\dot{s} = f - b\hat{b}^{-1}\hat{f} + (1 - \hat{b}b^{-1})(-\ddot{x}_d + \lambda\dot{\tilde{x}}) - (|f - b\hat{b}^{-1}\hat{f} + (1 - \hat{b}b^{-1})(-\ddot{x}_d + \lambda\dot{\tilde{x}})| + \eta)(s/\Phi)
\tag{4.18}
$$

which can be rewritten as:

$$
\dot{s} = w - (|w| + \eta)(s/\Phi)
\tag{4.19}
$$

Then

$$
\begin{aligned}
\frac{1}{2}\frac{d}{dt}(s^2) &= \dot{s}s = (w - (|w| + \eta)(s/\Phi))s \\
&\leq |ws| - ((|w| + \eta)\left|\frac{s}{\Phi}\right||s| \\
&< -\eta|s| < 0
\end{aligned}
\tag{4.20}
$$

Therefore, (4.17) and (4.20) imply that no matter what initial condition is, we always have

$$\frac{1}{2}\frac{d}{dt}s^2 = s\dot{s} \leq -\eta|s| < 0 \tag{4.21}$$

Consider an arbitrary point $(x, \dot{x})$ and let t_{reach} be the time taken for the system trajectory to reach the surface from this point. Integrating (4.21) from $t = 0$ to t_{reach} and considering initial points $(x, \dot{x})$ outside $B(t)$ results in

$$t_{reach} \leq \frac{1}{\eta}|s(0)| \tag{4.22}$$

It can be conclude from (4.22) that from any initial state $(x, \dot{x})$, the control law forces the state trajectory to reach the surface in a finite time.

Furthermore, from (4.4), it leads

$$s = \frac{d}{dt}\tilde{x} + \lambda\tilde{x} = (\frac{d}{dt} + \lambda)\tilde{x} \tag{4.23}$$

Letting $p = \frac{d}{dt}$, then

$$\tilde{x} = \left(\frac{1}{p + \lambda}\right)s \tag{4.24}$$

Therefore

$$\forall t \geq 0, \quad \tilde{x}(t) = \int_0^t e^{-\lambda(t-T)}s(T)dT \tag{4.25}$$

Since $|s(t)| \leq \Phi$, this implies

$$\forall t \geq 0, \quad \left| \tilde{x}(t) \right| \leq \Phi \int_0^t e^{-\lambda(t-T)} dT = (\Phi / \lambda)(1 - e^{-\lambda t}) \leq \Phi / \lambda \qquad (4.26)$$

It can be concluded from (4.26), that the state trajectory, once reaching the sliding surface, remains inside a neighborhood of the desired trajectory.

Therefore, the state trajectory reaches the boundary layer in a finite time no matter what initial state is and stays inside it for all later time. Hence, asymptotic tracking within a guaranteed accuracy is obtained in spite of modeling errors.

Chattering Phenomenon

Since it is undesirable for the control action to be switched at high frequencies, the ideal sliding mode control law is impractical in practice. Due to switching imperfections such as the bandwidth limit of switching, switching time delays and small time constants in the actuators, the discontinuity in the feedback control causes high frequency oscillation in the vicinity of the surface. This is the phenomenon of chattering.

Since chattering involves high control activity and may excite unmodeled high frequency dynamics, chattering degrades the system performance and may even lead to instability. In addition, chattering could cause high wear of moving mechanical components and bring high heat losses in electrical power circuits. Chattering is obviously undesirable in practice. Therefore, the solution of the chattering problem is very important when implementing a sliding mode controller in a real life system.

To mitigate chattering, the ideal sliding control law is modified to include a "boundary layer" about the sliding surface. Instead of switching discontinuously across the sliding surface, the control is linear inside the boundary layer. The

boundary layer eliminates chattering at the expense of greater tracking error.

4.2 FUZZY CONTROL

Fuzzy logic is a method of machine reasoning that recognizes degrees of truth rather than simple true and false values. Since fuzzy logic incorporates human knowledge and intelligence, it has strong learning and cognitive ability and good tolerance to uncertainty and imprecision. Conventional model-based control involves precise mathematical modeling of a system's dynamics. That is, a model-based control law can only work well by the prerequisite that the model does meet the requirements of accuracy. However, for systems like robotics applications that are very complicated, highly nonlinear, and with parameter uncertainty, conventional control methods are frequently inadequate. The fuzzy logic-based approach to solving such control problems has been found to be superior to conventional control methods in such cases.

A fuzzy logic controller is generally considered as an expert system that exploits fuzzy logic to analyze input to output performance. Essentially, it specifies a linguistic control strategy from expert knowledge. In fuzzy control, nonlinearity is handled by rules, membership functions, and the inference process. As a result, by using fuzzy logic, designers can realize lower costs and better system performance.

A fuzzy logic controller normally consists of three stages: an input stage, a processing stage, and an output stage. The input stage maps inputs into fuzzy sets. The processing stage maps input fuzzy sets into output fuzzy sets using a rule base, which is a set of linguistic rules describing the controller's operation. Finally, the output stage converts the output fuzzy sets acquired in the processing stage back into a crisp output value using defuzzification.

Among these three stages, the processing stage is the most important.

Depending on the practical situation, it contains logical rules in the form of IF-THEN statements, where the IF part is called the "premise" and the THEN part is called the "consequent."   In practice, the fuzzy rules usually have several parts to the premise that are combined using fuzzy operators, such as AND, OR, and NOT.   The total number of fuzzy sets depends on how to appropriately cover the universe of discourse of an input value while the shapes of the membership functions depend on the nature of the variables they specify.   Typical shapes commonly used as membership functions are triangular, trapezoidal, and Gaussian.

For the defuzzification, several different methods are available to obtain a crisp value from the output fuzzy sets.   One of the most common and simplest is the center-average inference method, in which the output membership function is tempered by the truth value of the premise.   Another commonly used method is the center of gravity method, in which the center of gravity of all output fuzzy sets is calculated to obtain the crisp output.

Since fuzzy control exploits natural language to mimic human logic, it has proved to be better for sorting and handling data than traditional nonfuzzy methods and has been proven an excellent choice for many control system applications

4.3   INTEGRAL CONTROL

Integral control computes the error between actual and desired output and integrates this error.   With integral action, the controller output is proportional to the amount of time the error is present as well as its magnitude, hence ideally the steady state error for a closed-loop integral control system is zero.   However, integral control responds relatively slowly to an error signal and can initially allow a large tracking errors.   This could lead to system instability and cyclic operation. Therefore, integral control is normally implemented in combination with other control

methods instead of being used alone.

CHAPTER V

BASIC STATE FEEDBACK CONTROL OF PNEUMATIC MUSCLE

5.1. DYNAMICAL BEHAVIOR OF PNEUMATIC MUSCLE

Most biological materials display gradual deformation and recovery, i.e. viscoelastic behavior, when loaded and unloaded respectively. Therefore, viscoelastic models are often exploited to describe dynamics of muscle. In the model, a spring and dashpot are usually used to simulate the properties of elasticity and viscosity, respectively. More in detail, the spring causes deformation proportional to the payload at any instance while the dashpot deforms proportional to the velocity of the load.

The properties of a pneumatic muscle system were studied in the Human Sensory Feedback Laboratory at Wright Patterson Air Force Base, Dayton, Ohio [41]. This particular PM has an inner bladder made from a section of 22.2 mm diameter bicycle tubing enclosed in a helically-wound nylon sheath used for supporting electrical cables. The unstretched, uncompressed diameter of the sheath is 31.75 mm. The PM is inflated by supplying voltage to a solenoid that controls the flow of pressurized gas into the rubber bladder. It is deflated by exciting another solenoid venting the contents of the bladder to the atmosphere. When inflated, the PM shortens due to the braided plastic sheath. Figures 5 and 6 show a PM hanging vertically actuating a mass [41, 48].

This PM system was investigated using an apparatus that allows precise actuation pressure control by a linear servo-valve. The length of the PM was

measured by a linear potentiometer.
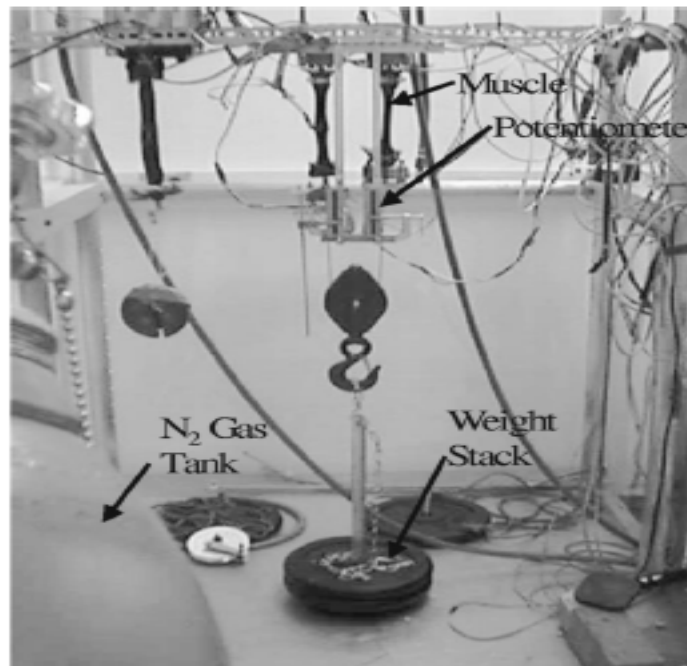
Figure 5 - Experimental apparatus for a PM actuating a mass.
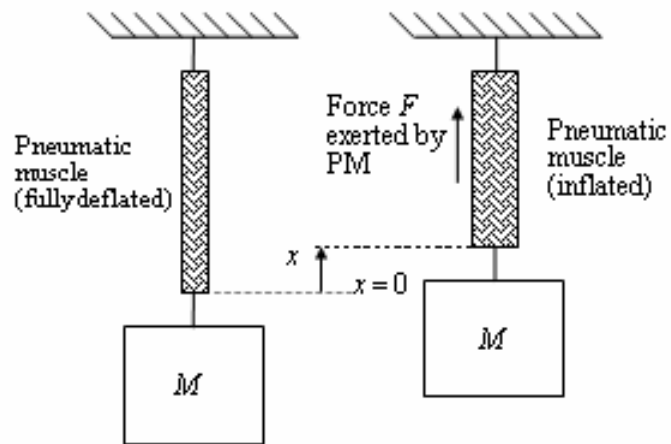
Figure 6 - Equivalent diagram for a PM actuating a mass.

The dynamic behavior of this PM system is modeled as a parallel arrangement of a contractile element $F(P)$, spring element $K(P)$, and damping element $B(P)$ (see Figure 7). All three elements have pressure-dependent

coefficients. This pressure can be commanded externally by varying the voltage supplied to the inlet valve.
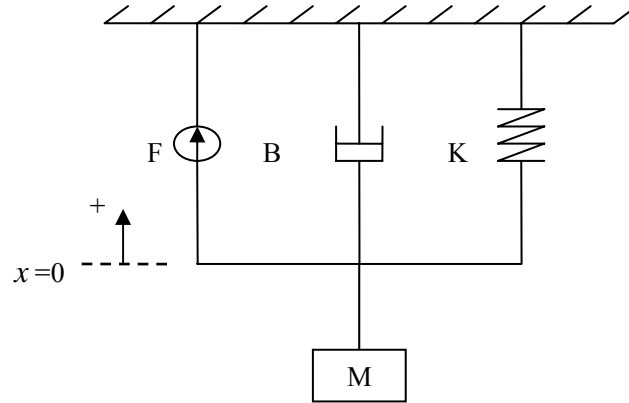
Figure 7 - Three-element model of the PM actuating a mass

Let x be the amount of PM contraction, with $x = 0$ corresponding to the PM being fully deflated and extended and x increasing as the PM contracts. Let $P(t)$ indicate the pressure in the supply line of PM. Then the dynamical equation for the system of Figure 7 is

$$M\ddot{x} + B(P(t))\dot{x} + K(P(t))x = F(P(t)) - Mg \qquad (5.1)$$

where M is the load mass, g is the acceleration of gravity, and $F(P), K(P), B(P)$ are the contractile coefficient, spring coefficient, damping coefficient respectively, which are given in [41] as:

$$
\begin{aligned}
F(P(t)) &= F_0 + F_1 P(t) = 179.2 + 1.39 P(t) \,(\text{N}) \\
K(P(t)) &= K_0 + K_1 P(t) = 5.71 + 0.0307 P(t) \,(\text{N/m}) \\
B(P(t)) &= B_0 + B_1 P(t) = 1.01 + 0.00691 P(t) \,(\text{N-s/m}) \,\text{inflation} \\
B(P(t)) &= B_0 + B_1 P(t) = 0.6 - 0.000803 P(t) \,(\text{N-s/m}) \,\text{deflation}
\end{aligned}
\qquad (5.2)
$$

33

The actuation pressure $P(t)$ applied to the model must remain within the range

206.8 – 620.5 kPa (30 -90 psi) for the coefficients in (5.2) to be valid.

From (5.1), the total force exerted by the PM on the mass is

$F(P(t)) - B(P(t))\dot{x} - K(P(t))x$. If several PMs are present, each one generally has

its own actuation pressure $P(t)$ hence its own $F(P(t)), K(P(t)), B(P(t))$ coefficients,

and its own inflation or deflation status. Note that for the PM model (5.1), the input

is actuation pressure $P(t)$, which enters into the model through the PM coefficients.

First, investigate the stability of the system of Figure 6 under simple linear

state feedback.

Theorem 2: There is a linear state feedback control law which locally

stabilizes the PM lifting a mass described by (5.1).

Proof: Substituting (5.2) into (5.1) yields:

$$\ddot{x} = -((B_0 + B_1 P)\dot{x} + (K_0 + K_1 P)x)/M + (F_0 + F_1 P)/M - g \qquad (5.3)$$

Defining states $x_1 = x, \ x_2 = \dot{x}$, (5.3) can be rewritten as:

$$\dot{X} = f(x_1, x_2, P) \qquad (5.4)$$

where

$$X = [x_1 \ x_2]^T \qquad (5.5a)$$

$$f = [x_2 \quad -((B_0 + B_1 P)x_2 + (K_0 + K_1 P)x_1)/M + (F_0 + F_1 P)/M - g]^T \qquad (5.5b)$$

In order to transform the equilibrium point to the origin of the state space, let

$$y = x - \frac{F_0 - Mg}{K_0} \quad \text{and define} \quad y_1 = y, \ y_2 = \dot{y}. \quad \text{Then defining} \quad Y = [y_1 \quad y_2]^T, \ (5.4)$$

becomes:

$$\dot{Y} = f(y_1 + \frac{F_0 - Mg}{K_0}, y_2, P) \tag{5.6}$$

Linearizing (5.6) at the equilibrium point $[y_1 \quad y_2]^T = [0, \ 0]^T$ and $P = 0$, we obtain:

$$\dot{Y} = AY + BP \tag{5.7}$$

where

$$A = \begin{bmatrix} 0 & 1 \\ -\dfrac{K_0}{M} & -\dfrac{B_0}{M} \end{bmatrix} \tag{5.8a}$$

$$B = \begin{bmatrix} 0 \\ \dfrac{F_1}{M} - \dfrac{K_1 F_0 - K_1 Mg}{MK_0} \end{bmatrix} \tag{5.8b}$$

Now consider the linear state feedback control law:

$$P = GY = y_1 + cy_2 \tag{5.9}$$

where

$$G = \begin{bmatrix} c & 1 \end{bmatrix} \tag{5.10}$$

and c is a real constant.

Now, the closed-loop dynamics can be linearly approximated as:

$$\dot{Y} = DY = (A + BG)Y \tag{5.11}$$

where

$$D = \begin{bmatrix} d_{11} & d_{12} \\ d_{21} & d_{22} \end{bmatrix} = \begin{bmatrix} 0 & 1 \\ \dfrac{F_1}{M} - \dfrac{K_1 F_0 - K_1 Mg}{MK_0} - \dfrac{K_0}{M} & c\left(\dfrac{F_1}{M} - \dfrac{K_1 F_0 - K_1 Mg}{MK_0}\right) - \dfrac{B_0}{M} \end{bmatrix} \tag{5.12}$$

It is straightforward to show that the eigenvalues of D are

$$\lambda_{1,2} = \frac{1}{2}\left[d_{11} + d_{22} \pm \sqrt{4d_{12}d_{21} + (d_{11} - d_{22})^2} \right] \tag{5.13}$$

Substituting (5.2) into (5.13), we have

$$\lambda_{1,2} = \frac{1}{2}\left[\frac{0.427c - B_0}{M} + 0.0527c \pm \sqrt{4\left(\frac{-5.283}{M} + 0.0527\right) + \left(\frac{0.427c - B_0}{M} + 0.0527c\right)^2} \right] \tag{5.14}$$

It can be verified that $\lambda_{1,2}$ are strictly in the left-half complex plane provided:

$$\begin{cases} \dfrac{0.427c - B_0}{M} + 0.0527c < 0 \\ 4\left(\dfrac{-5.283}{M} + 0.0527\right) < 0 \end{cases} \tag{5.15}$$

Choosing the worst case for B_0, i.e. $B_0 = 0.6$, and $c = 0.1$, (5.15) leads to:

$$M < 100.2\text{kg} \tag{5.16}$$

Referring to [41], the maximum load applied to the system is 898/9.8= 91.6Kg,

which satisfies (5.16).   Thus, as long as (5.16) is satisfied, the linearized system (5.11) is stabilized with the linear state feedback law (5.9).

Therefore, by Lyapunov's indirect (linearization) method, we also have that the equilibrium point $[y_1 \ y_2]^T = [0, \ 0]^T$ is (locally) asymptotically stable for the actual nonlinear system (5.6), i.e., $[x_1 \ x_2]^T = [\dfrac{F_0 - Mg}{K_0}, \ 0]^T$ is asymptotically stable for the original nonlinear system (5.4).

5.2. EFFECT OF HEAT ON PNEUMATIC MUSCLE

Heating is an important factor which could affect the dynamical behavior (model parameters) of PM systems.   PM is prone to suffer the effect of heating because the key component inside pneumatic muscle is a rubber bladder, which is also well known to be insulated and poor at heat transfer.   During the repetitive operation of inflation and deflation, the inner rubber bladder generates elastic deformation frequently.   A loss of energy occurs along with this process, which results in heating of the rubber.   The generated heat energy is difficult to emit out from the rubber hence it accumulates, which makes the temperature of the rubber bladder rise throughout the process of operation.   As a result, the mechanical capability of the pneumatic muscle degrades, i.e., the friction between the outer sheath and the rubber bladder is lessened as well as thickness of the rubber ladder.   As a consequence, the spring capability is reduced.   In addition, both contractile force and damping ratio are lessened.   Hence, the characteristics of PMs change if the PMs are operated for an extended period of time.   In other words, all related coefficients of the PM i.e. F_0, F_1 etc. in (5.2) are assumed to decrease slowly when the PM is operated for an extended time.

CHAPTER VI

SLIDING MODE TRACKING CONTROL OF A ONE-JOINTMANIPULATOR WITH PMS IN BICEP/TRICEP CONFIGURATION

6.1 MODELING OF A ONE-JOINT LIMB WITH PM IN BICEP/TRICEP CONFIGURATION

As stated in [41], the physical and modeling properties of a certain kind of pneumatic muscle (PM) have been studied at the Human Sensory Feedback Laboratory in Wright Patterson Air Force Base, Dayton, Ohio. Research indicates that a three-element model can describe the dynamics of PM. The PM system was investigated using an apparatus that allowed precise actuation pressure control by a linear servo-valve, meanwhile, length change of the PM was measured by a linear potentiometer. The results showed that the PM could be represented as a model with contractile element, spring element, and damping element in parallel. All three elements have pressure-dependent coefficients for actuation pressure in the range 206.8 – 620.5 kPa (30 - 90 psi).

Figure 8 shows an anthropomorphic arm actuating a mass, with PMs in the position of a bicep/tricep pair [46]. The upper arm remains stationary as the PMs expand and contract, moving the forearm. The upper ends of the bicep and tricep are attached to a motionless reference point. The mass is held at the end of the forearm (i.e. hand). The forearm, which is considered massless, is attached to the upper arm by a frictionless planar revolution joint. The PMs are attached to the forearm at point A, which is a distance a from the joint. The distance from the center of mass of the load to the joint is L.
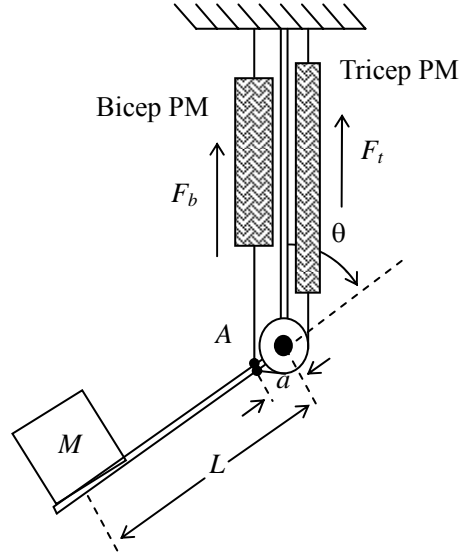
Figure 8 - Single-joint planar manipulator with PMs in bicep/tricep configuration

The forearm is free to rotate through an angle θ, where $\theta = 0°$ corresponds to the tricep being fully shortened while bicep is fully lengthened, and $\theta = 180°$ corresponds to the tricep being fully lengthened while the bicep is fully shortened. For simplicity, the PM force is assumed to always act parallel to the forearm. This is valid as long as θ is not close to either of its extremes.

Let subscripts b denote bicep PM coefficients and subscripts t denote tricep PM coefficients. Also, let x_b denote bicep PM length and x_t denote tricep PM length. Since the total clockwise torque exerted by the bicep on the elbow is $(F_b - B_b \dot{x}_b - K_b x_b)a \sin \theta$, the total counterclockwise torque exerted by the tricep on the elbow is $(F_t - B_t \dot{x}_t - K_t x_t)r$ and the counterclockwise torque imparted to the elbow by gravity is $MgL \sin \theta$, the dynamics of the system of Figure 8 are described by:

$$I\ddot{\theta} = (F_b - B_b \dot{x}_b - K_b x_b)a \sin \theta - (F_t - B_t \dot{x}_t - K_t x_t)r - MgL \sin \theta \qquad (6.1)$$

where $I = ML^2$ is the moment of inertia of the mass about the elbow and g is the acceleration of gravity. Note that, since the bicep force is multiplied by $a \sin \theta$ the bicep loses controllability at $\theta = 0°$ and $\theta = 180°$. Thus, the arm should be kept away from these extremes. The tricep does not have this limitation because its cable always makes an angle of $\alpha = \sin^{-1}\left(r/a\right)$ with the arm regardless of θ.

As shown in (5.2), we use $F = F_0 + F_1 P$, $K = K_0 + K_1 P$, and $B = B_0 + B_1 P$ where $F_1 = 1.39$, $K_0 = 5.71$, $K_1 = 0.0307$, and B_0, B_1 depend on whether the PM in question is being inflated or deflated [41], as follows:

$$B_0 = \begin{cases} 1.01, \text{ inflation} \\ 0.6, \text{ deflation} \end{cases}, \quad B_1 = \begin{cases} 0.00691, \text{ inflation} \\ -0.000803, \text{ deflation} \end{cases} \tag{6.2}$$

The internal bicep and tricep pressures P_b and P_t are the control variables that can be independently commanded by the controller as inputs to the system. Thus this is a 2-input system. Note that the PM dynamics depend on whether the PM is being inflated or deflated. Obviously, (6.1) is in an unusual form for control since the control inputs enter into the system through the coefficients F, B, and K and not as a separate term.

To convert this 2-input system to a single-input system, it is assumed that the bicep and tricep internal pressures are given by

$$P_b = P_0 + \Delta p \tag{6.3a}$$

$$P_t = P_0 - \Delta p \tag{6.3b}$$

where P_0 is a nominal constant pressure and Δp is the change in pressure which is now the independent control input. Note that, with PM pressure defined as in (6.3), one PM inflating always corresponds to the other deflating. Therefore, one set of B

parameters (say inflation) will apply to one of the PMs while the other set (deflation) applies to the other PM at a given time. When the inflation status of the PMs changes, they trade B parameters. We denote the bicep B coefficients as B_{0b} and B_{1b}, and the tricep B coefficients as B_{0t} and B_{1t}.

When either PM is fully lengthened, its length is defined as zero, and when it is fully shortened, its length is defined as $-2a$ (i.e. x is the amount of PM shortening). Therefore, from Figure 8, the bicep length is $x_b = a(\cos\theta - 1)$ and the tricep length is $x_t = -a(1 + \cos\theta)$. Combining (6.1) with the above relationships for F, B, and K, the following 2nd order equation is obtained to describe the system of Figure 8:

$$\ddot{\theta} = f(\theta, \dot{\theta}) + b(\theta, \dot{\theta})\Delta p \tag{6.4}$$

where

$$f(\theta, \dot{\theta}) = \sum_{i=1}^{6} c_i f_i(\theta, \dot{\theta}) \tag{6.5a}$$

$$b(\theta, \dot{\theta}) = \sum_{i=1}^{6} d_i f_i(\theta, \dot{\theta}) \tag{6.5b}$$

In (6.5), $f_1 = \sin\theta$, $f_2 = \sin\theta(\cos\theta - 1)$, $f_3 = \dot{\theta}\sin^2\theta$, $f_4 = 1$, $f_5 = 1 + \cos\theta$, $f_6 = \dot{\theta}\sin\theta$, $c_1 = (aF_0 + aF_1 P_0 - MgL)/I$, $c_2 = (K_0 + K_1 P_0)a^2/I$, $c_3 = (-B_{0b} - B_{1b}P_0)a^2/I$, $c_4 = -(F_1 P_0 + F_0)r/I$, $c_5 = (K_0 + K_1 P_0)ar/I$, $c_6 = (-B_{0t} - B_{1t}P_0)ar/I$, $d_1 = F_1 a/I$, $d_2 = K_1 a^2/I$, $d_3 = -B_{1b}a^2/I$, $d_4 = F_1 r/I$, $d_5 = -K_1 ar/I$, and $d_6 = B_{1t}ar/I$.

The model (6.1) is now in a form suitable for sliding mode control (4.1).

6.2 SLIDING MODE CONTROL FOR PLANAR LIMB MODEL

Due to the imperfect knowledge of coefficients F_0, F_1, K_0, K_1, B_0, and B_1, $f(\theta,\dot{\theta})$ and $b(\theta,\dot{\theta})$ in (6.4) must be assumed to be imprecise. Assume the extent of the imprecision on $f(\theta,\dot{\theta})$ can be bounded by a known continuous function of θ and $\dot{\theta}$ and that the extent of the imprecision on $b(\theta,\dot{\theta})$ can be bounded by a known, continuous function of θ and $\dot{\theta}$ as described in Chapter 4. The control problem is to get the joint angle $\theta(t)$ to track a desired trajectory $\theta_d(t)$ in the presence of model imprecision on $f(\theta,\dot{\theta})$ and $b(\theta,\dot{\theta})$. Then the following result is acquired concerning sliding mode control of the single joint planar arm system [64].

Theorem 3: Consider the single-joint planar arm system of Figure 8, modeled by (6.4). Let $\hat{f}(\theta,\dot{\theta})$ and $\hat{b}(\theta,\dot{\theta})$ be approximations of f and b as described in Chapter 4. Then, the sliding mode control

$$\Delta p(t) = (-\hat{f} + \theta_d - \lambda\dot{\tilde{\theta}} - k\mathrm{sat}(s/\Phi))\hat{b}^{-1} \tag{6.6}$$

results in tracking error which is bounded by

$$\lim_{t_0 \to \infty} \sup_{t \geq t_0} \left|\theta(t) - \theta_d(t)\right| \leq \frac{\Phi}{\lambda} \tag{6.7}$$

where Φ and λ are arbitrary positive constants. Furthermore, the control effort is bounded by

$$\lim_{t_0 \to \infty} \sup_{t \geq t_0} \left|\Delta p(t)\right| \leq \frac{-\inf(\hat{f}) + \sup(\theta_d) + 2\lambda\Phi}{\inf(\hat{b})} \tag{6.8}$$

Proof: The bound on tracking error (6.7) is direct from Theorem 1 in Chapter 4. The bound on control effort is a straightforward consequence of (6.8), (4.5), and (4.6).

6.3   SIMULATION RESULTS

The system of Figure 8 with PMs in bicep/tricep pair configuration is simulated using a 4th-order Runge-Kutta algorithm with a step size of 0.01seconds. Let $L = 0.46$ m , $a = 7.62$ cm, $M = 14.6$ kg, and $r = 5.08$ cm.   Since $a = 7.62$ cm, the full travel of the forearm from $\theta = 0$ (arm fully straightened) to $\theta = \pi$ (arm fully bent) corresponds to a maximum change in length of the PM of 15.24 cm.

First, consider the desired trajectory for the joint:

$$\theta_d(t) = \frac{\pi}{2} + 0.5(\sin(2\pi f_1 t) + \sin(2\pi f_2 t) + \sin(2\pi f_3 t)) \qquad (6.9)$$

with $f_1 = 0.02\text{Hz}, f_2 = 0.05\text{Hz},$ and $f_3 = 0.09\text{Hz}.$ This trajectory spans joint angles from approximately $30°$ to $150°$ during the time period $t = 0 - 60$ sec.

Let $\lambda = 10$ and $\eta = 10$ (chosen by trial and error to yield good performance). The chosen boundary layer thickness is $\Phi = 1$.   From Theorem 3, $\varepsilon = \frac{\Phi}{\lambda}$ is the guaranteed tracking precision.   Therefore, for this simulation we have $\varepsilon = 0.1$.

Assume that the true values of $f(\theta, \dot{\theta})$ and $b(\theta, \dot{\theta})$ in (6.4) are known to fall within $\pm 30\%$ of the best estimates we have of them, i.e. $\hat{f}(\theta, \dot{\theta})$ and $\hat{b}(\theta, \dot{\theta})$. Then we have $F = 0.3|\hat{f}|$, $b_{\max} = 1.3\hat{b}$, $b_{\min} = 0.7\hat{b}$, and the gain margin β is determined as 1.86 from (4.3b).

The sliding control input to the PM is given in (6.6) with parameters defined as above.   For the simulation, the actual $f(\theta, \dot{\theta})$ and $b(\theta, \dot{\theta})$ terms were randomly chosen to lie within $\pm 30\%$ of their modeled values.   Figure 9 shows the tracking errors for three different sets of f and b within this range.   It is seen that for all systems the tracking error is within predicted bounds, with areas of maximum error

corresponding to $\dot{\theta}$ changing signs, i.e. places where the arm motion has to change direction. This is especially noticeable when the arm must change from a downward motion to an upward motion.

Figure 10 shows a typical control effort Δp with $P_0 = 344.7\,\text{kpa}$. It is evident that input pressure varies smoothly without any obvious chattering. Therefore, by using the sliding mode controller, the PM system achieves desired performance with good tracking precision and no obvious chattering for all three systems which may represent the true arm with PMs in bicep/tricep pair configuration.

Figure 9 - Tracking errors for three possible actual arms, $M = 14.6\text{kg}$
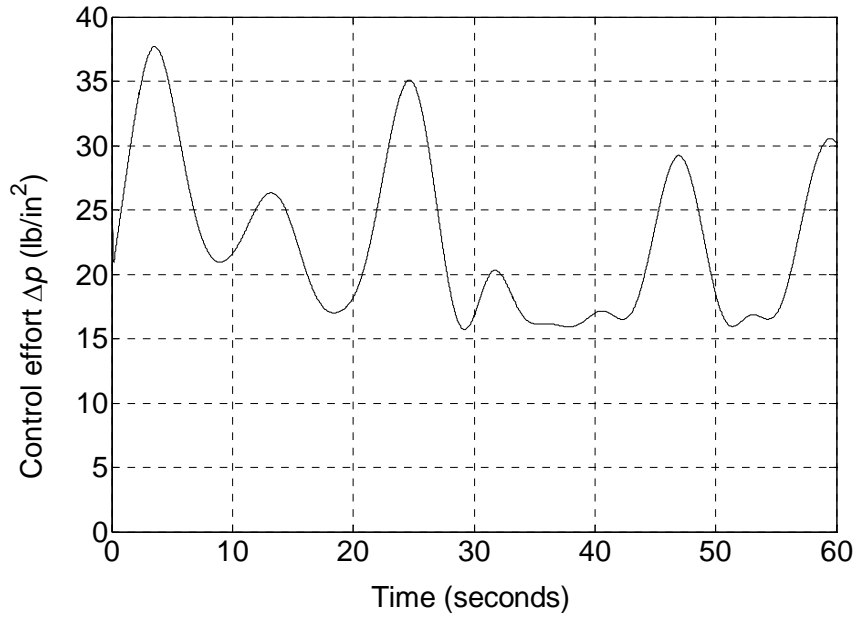
Figure 10 - Typical control effort Δp, $M = 14.6\text{kg}$

To investigate the robustness of the sliding controller to changing masses, we increased the mass M to 29.2 kg, i.e. an increase of 100%. Figure 11 shows tracking errors for three different actual arms randomly chosen within the $\pm 30\%$ range. Tracking is again within predicted bounds. Figure 12 shows a typical control effort when $M = 29.2\,\text{kg}$. Note that the control effort is larger than the $M = 14.6$ kg case, which is to be expected since a heavier mass is being moved. The mass M could be increased more, but very heavy masses require the input pressure to be outside the allowed range of PM internal pressure $206.8 - 620.5$ kPa. This limitation is not the sliding controller's shortcoming however; it is merely an acknowledgement that the PM internal pressure must be kept within reasonable bounds to protect against actuator failure (bursting). If more force is desired, several PMs can always be placed in parallel.

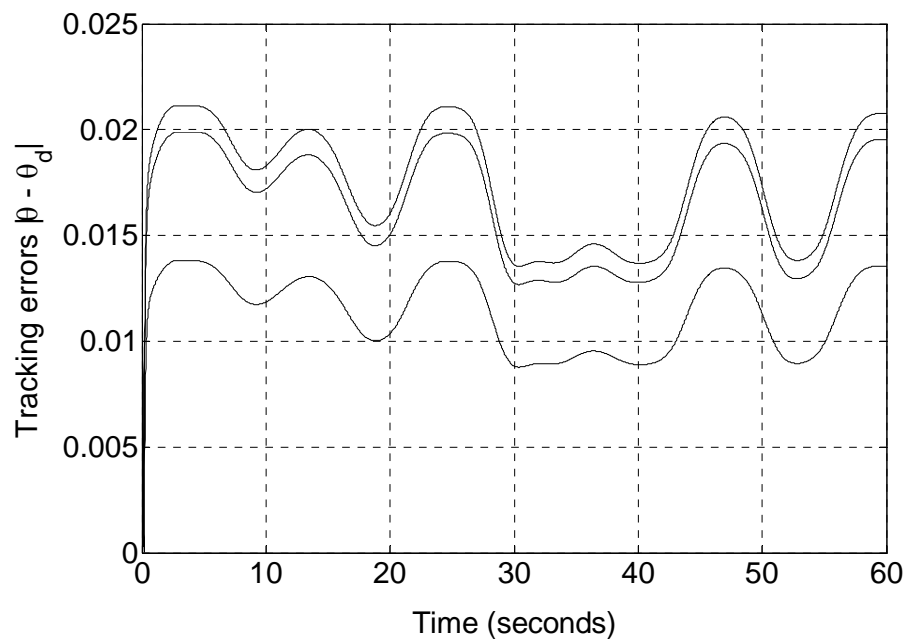Figure 11 - Tracking errors for three possible actual arms, $M = 29.2\text{kg}$

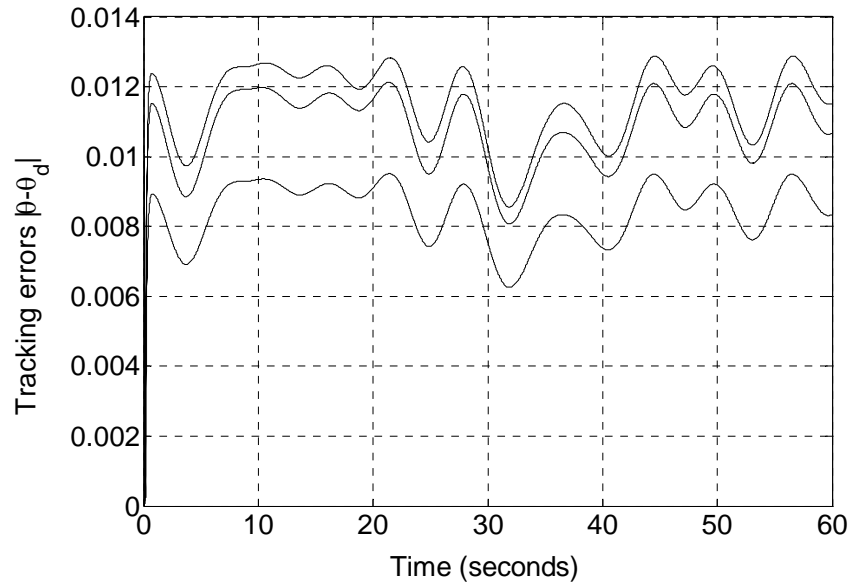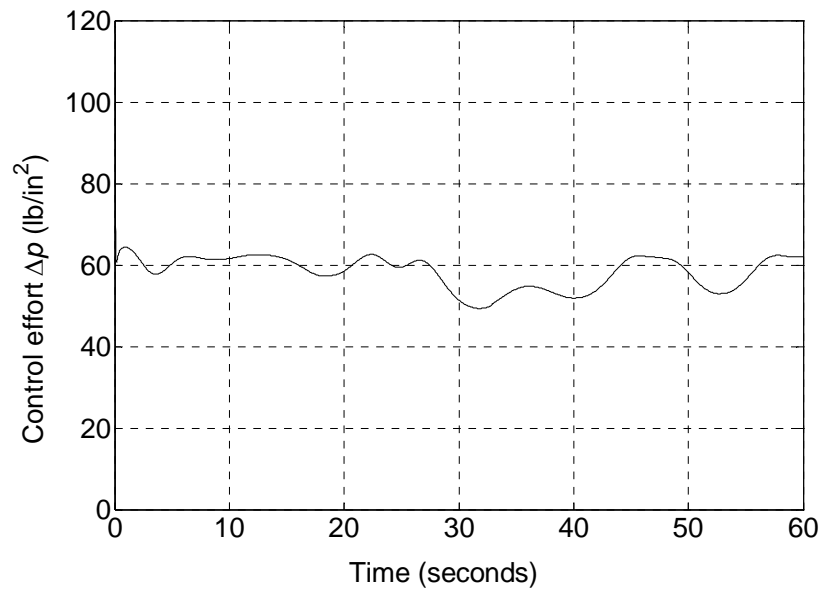Figure 12 - Typical control effort Δp, $M = 29.2\,\text{kg}$

It is noted from Figure 12 that since $P_0 = 344.7\,\text{kpa}$, the values of Δp would

require tricep pressure P_t to be negative (6.5b). This is impossible, and in such a case, $P_t = 0$ is simply set. The simulation reflects this. The fact that tricep pressure is mostly zero when $M = 29.2\,\text{kg}$ results from the heavier mass exerting enough downward force to track the downward parts of the reference trajectory without needing the tricep to help pull the arm down.

To further verify the sliding mode controller, another simulation is performed to track a pseudo-square wave signal with a typical system within the $\pm 30\%$ range. Here, the desired trajectory is

$$\theta_d(t) = \begin{cases} \dfrac{3}{4}\pi, & \sin(2\pi f(t-3)) \geq \dfrac{1}{4} \\ \dfrac{\pi}{2} + \pi \sin\left(2\pi f(t-3)\right), & \left|\sin(2\pi f(t-3))\right| \leq \dfrac{1}{4} \\ \dfrac{1}{4}\pi, & \sin(2\pi f(t-3)) \leq -\dfrac{1}{4} \end{cases} \qquad (6.10)$$

with $f = 0.1\text{Hz}$. This function transitions between constant values of $\pi/4$ and $3\pi/4$ smoothly rather than with discontinuous jumps. For the design parameters, we used $\lambda = 10$, $\eta = 10$, and $\Phi = 0.3$. Therefore, the tracking accuracy is $\varepsilon = \dfrac{\Phi}{\lambda} = 0.03$.

From Figure 13, the joint angle trajectory is seen to follow the desired one with acceptable error except at the times of rapid transition between the two constant values. This is attributed to the fact that in the simulation the PM pressures are constrained to lie within the range 206.8 – 620.5 kPa to better conform to actual PM operation. Therefore, the needed input pressure dictated by the sliding mode controller is not applied and tracking accuracy is lost.
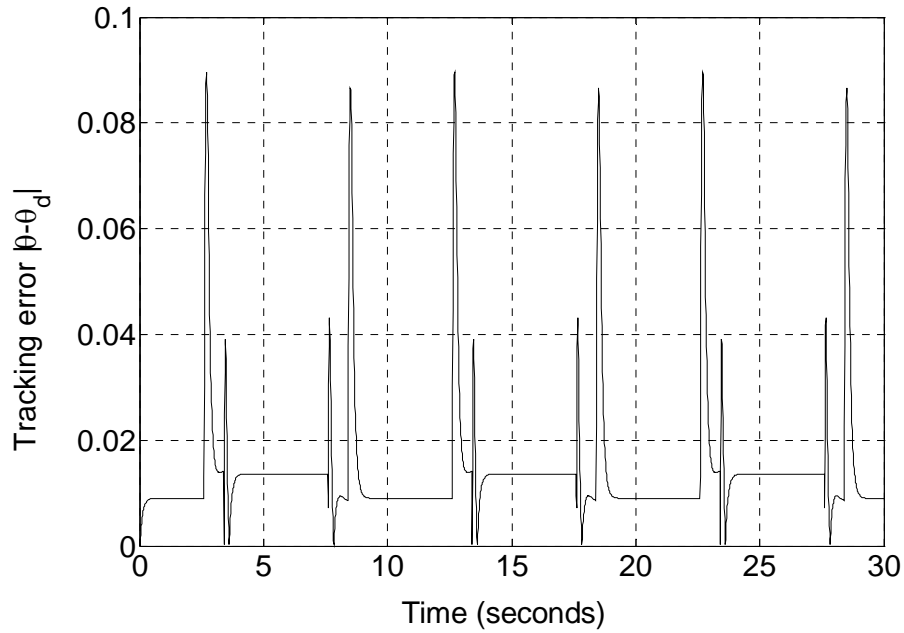
Figure 13 - Tracking error (pseudo-square wave)

6.4 DISCUSSION

The one-joint limb system actuated by PM in bicep/tricep pair is essentially with nonlinear and time-varying parameters. Sliding mode control methods have been applied to this problem since fixed structure controllers are less robust to parameter changes than sliding mode ones. In the case of time-invariant and well-known coefficients, traditional methods, i.e. PID may give good results. However, if coefficients or physical quantities change significantly, the fixed PID cannot stabilize the system. Assuming certain degrees of inaccuracy in the knowledge of the PM coefficients, a sliding mode controller was designed. In order to eliminate chattering, the control action was also designed to be smoothed to achieve a trade-off between control bandwidth and tracking precision. With the sliding mode controller given, good tracking performance is obtained even in the presence of modeling uncertainties. The two trajectories considered are used because they mimic two common working situations of the PMs. Trajectory (6.9) represents a movement of the mass in a smooth trajectory. Trajectory (6.10) represents the task of holding the mass in a stationary

position and then lifting it up or dropping it down suddenly. Simulation results demonstrate the effectiveness of sliding mode control for PM applications.

In both cases, the sliding mode controller can work with desirable performance of good tracking precision and little chattering.

CHAPTER VII

FUZZY SLIDING MODE TRACKING CONTROL
OF A TWO-JOINT MANIPULATOR ACTUATED BY FOUR PM GROUPS

7.1   MODELING OF A TWO-JOINT MANIPULATOR ACTUATED BY FOUR PM GROUPS

To further investigate the effectiveness of sliding mode control approach, consider the planar arm manipulator [57] shown in Figure 14.
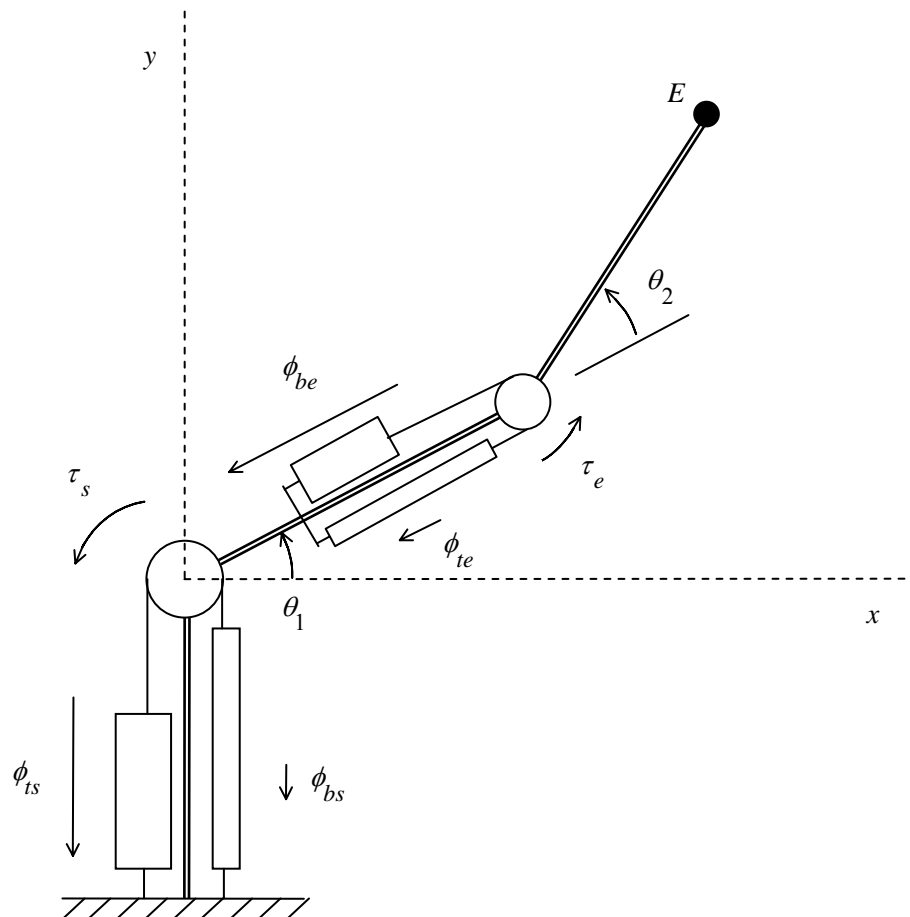
Figure 14 - Planar arm actuated by four PM group

Assume there are n_s pairs of matched PMs (i.e. all PMs have identical coefficients)

tied together around the shoulder pulley with all tricep PMs receiving the same input

pressure P_{ts} and all bicep PMs receiving the same input pressure P_{bs}. Similarly,

assume there are n_e pairs of matched PMs tied together around the elbow pulley

with all tricep PMs receiving the same input pressure P_{te} and all bicep PMs

receiving the same input pressure P_{be}. The elbow PMs are not assumed to be

matched with the shoulder PMs.

Under these conditions, the shoulder and elbow torques τ_s and τ_e can be

expressed as:

$$\tau_s = n_s (F_s - K_s x_{ts} - B_{ts} \dot{x}_{ts} - F_s + K_s x_{bs} + B_{bs} \dot{x}_{bs}) r_s \qquad (7.1a)$$

$$\tau_e = n_e (F_e - K_e x_{be} - B_{be} \dot{x}_{be} - F_e + K_e x_{te} + B_{te} \dot{x}_{te}) r_e \qquad (7.1b)$$

where $F_s, K_s, B_{ts},$ and B_{bs} are the coefficients for the shoulder PMs,

F_e, K_e, B_{te} and B_{be} are the coefficients for the elbow PMs, t subscripts denote

tricep PM quantities, b subscripts denote bicep PM quantities, s subscripts denote

shoulder PM quantities, e subscripts denote elbow PM quantities and r denotes

pulley radius.

Let the shoulder PM input pressures be given by

$$P_{bs} = P_{0bs} + \Delta P_s \qquad (7.2a)$$

$$P_{ts} = P_{0ts} - \Delta P_s \qquad (7.2b)$$

where P_{0bs} and P_{0ts} are arbitrary positive nominal constant pressures and ΔP_s is

an arbitrary function of time that is commanded by the controller. With these

definitions, the set of n_s shoulder antagonist pairs becomes a single-input system

with input ΔP_s. When the bicep pressure increases, the tricep pressure decreases and

vice versa.

Similarly, let the inlet pressures of the elbow PMs be defined as:

$$P_{be} = P_{0be} + \Delta P_e \tag{7.3a}$$

$$P_{te} = P_{0te} - \Delta P_e \tag{7.3b}$$

where P_{0be} and P_{0te} are arbitrary positive nominal constant pressures and ΔP_e is an arbitrary function of time that is commanded by the controller. With these definitions, the set of n_e elbow antagonist pairs becomes a single-input system with input ΔP_e. Therefore, the 2-DOF two-joint planar manipulator becomes a 2-input system.

As addressed in [57], then the dynamical model for the planar arm actuated by four groups of PMs can be expressed as:

$$\begin{bmatrix} \ddot{\theta}_1 \\ \ddot{\theta}_2 \end{bmatrix} = D^{-1}\left(-C\begin{bmatrix} \dot{\theta}_1 \\ \dot{\theta}_2 \end{bmatrix} - \begin{bmatrix} f_1 \\ f_2 \end{bmatrix} + \begin{bmatrix} \tau_{0s} \\ \tau_{0e} \end{bmatrix}\right) + D^{-1}\begin{bmatrix} \tau_{1s} & 0 \\ 0 & \tau_{1e} \end{bmatrix}\begin{bmatrix} \Delta P_s \\ \Delta P_e \end{bmatrix} \tag{7.4}$$

where D is a 2×2 symmetric positive definite matrix:

$$D = \begin{bmatrix} d_{11} & d_{12} \\ d_{12} & d_{22} \end{bmatrix} \tag{7.5}$$

with

$$\begin{aligned} d_{11} &= 2m_1 l_{c1}^2 + m_2(l_1^2 + l_{c2}^2 + 2l_1 l_{c2}\cos\theta_2) + m_2 l_{c2}^2 \\ d_{12} &= m_2(l_{c2}^2 + l_1 l_{c2}\cos\theta_2) \\ d_{22} &= 2m_2 l_{c2}^2 \end{aligned} \tag{7.6}$$

and

$$C = \begin{bmatrix} c_{11} & c_{12} \\ c_{21} & c_{22} \end{bmatrix} \tag{7.7}$$

with

$$
\begin{aligned}
c_{11} &= -m_2 l_1 l_{c2} \sin\theta_2 \dot\theta_2 \\
c_{12} &= -m_2 l_1 l_{c2} \sin\theta_2 (\dot\theta_1 + \dot\theta_2) \\
c_{21} &= m_2 l_1 l_{c2} \sin\theta_2 \dot\theta_1 \\
c_{22} &= 0
\end{aligned}
\tag{7.8}
$$

and

$$
\begin{aligned}
f_1 &= (m_1 l_{c1} + m_2 l_1) g \cos\theta_1 + m_2 l_{c2} g \cos(\theta_1 + \theta_2) \\
f_2 &= m_2 l_{c2} g \cos(\theta_1 + \theta_2)
\end{aligned}
\tag{7.9}
$$

and

$$
\begin{aligned}
\tau_{0s} = n_s [&F_{0s} + F_{1s} P_{0ts} - (K_{0s} + K_{1s} P_{0ts}) x_{ts} - (B_{0ts} + B_{1ts} P_{0ts}) \dot{x}_{ts} - F_{0s} - F_{1s} P_{0bs} \\
&+ (K_{0s} + K_{1s} P_{0bs}) x_{bs} + (B_{0bs} + B_{1bs} P_{0bs}) \dot{x}_{bs}] r_s
\end{aligned}
$$

$$\tag{7.10a}$$

$$
\begin{aligned}
\tau_{0e} = n_e [&F_{0e} + F_{1e} P_{0be} - (K_{0e} + K_{1e} P_{0be}) x_{be} - (B_{0be} + B_{1be} P_{0be}) \dot{x}_{be} - F_{0e} - F_{1e} P_{0te} \\
&+ (K_{0e} + K_{1e} P_{0te}) x_{te} + (B_{0te} + B_{1te} P_{0te}) \dot{x}_{te}] r_e
\end{aligned}
$$

$$\tag{7.10b}$$

$$\tau_{1s} = n_s [-F_{1s} + K_{1s} x_{ts} - B_{1ts} \dot{x}_{ts} - F_{1s} + K_{1s} x_{bs} + B_{1bs} \dot{x}_{bs}] r_s \tag{7.10c}$$

$$\tau_{1e} = n_e [F_{1e} + K_{1e} x_{be} - B_{1be} \dot{x}_{be} + F_{1e} - K_{1e} x_{te} + B_{1te} \dot{x}_{te}] r_e \tag{7.10d}$$

In the above, $m_i, l_i,$ and l_{ci} are the mass, length, and location of center of mass of link i respectively ($i = 1$ for upper arm and $i = 2$ for forearm),

B_{0ts}, B_{1ts}, B_{0bs}, B_{1bs}, B_{0be}, B_{1be}, B_{0te}, and B_{1te} are the appropriate coefficients from (5.2), depending on whether the PMs are being inflated or deflated.

Defining

$$
\begin{bmatrix} a_1 \\ a_2 \end{bmatrix} = D^{-1}\left(-C\begin{bmatrix} \dot{\theta}_1 \\ \dot{\theta}_2 \end{bmatrix} - \begin{bmatrix} f_1 \\ f_2 \end{bmatrix} + \begin{bmatrix} \tau_{0s} \\ \tau_{0e} \end{bmatrix} \right)
$$
$$
G = \begin{bmatrix} g_{11} & g_{12} \\ g_{21} & g_{22} \end{bmatrix} = D^{-1}\begin{bmatrix} \tau_{1s} & 0 \\ 0 & \tau_{1e} \end{bmatrix}
$$

(7.11)

(7.4) can be written as:

$$
\begin{bmatrix} \ddot{\theta}_1 \\ \ddot{\theta}_2 \end{bmatrix} = \begin{bmatrix} a_1 \\ a_2 \end{bmatrix} + G\begin{bmatrix} \Delta P_s \\ \Delta P_e \end{bmatrix}
$$

(7.12)

The system (7.12) is a pair of second-order nonlinear equations with input vector $[\Delta P_s\ \Delta P_e]^T$ and is addressable via MIMO sliding-mode techniques. The differential pressures ΔP_s and ΔP_e can be commanded by the SMC outputs.

7.2   FUZZY SLIDING MODE TRACKING CONTROL OF A TWO-JOINT MANIPULATOR

It is very difficult to have perfect knowledge of coefficients $F, K,$ and B for all PMs. In addition, these coefficients change over time due to heating and cooling of the PM. Hence, $a_1, a_2,$ and G in (7.12) must be assumed imprecise. Let the extent of the imprecision on $a_1, a_2,$ and G be bounded by known continuous function of $\theta_1, \dot{\theta}_1, \theta_2, \dot{\theta}_2$. The control problem is to determine the input functions $\Delta P_s(t)$ and $\Delta P_e(t)$ to force the end effector E to follow a desired path in the spatial variables x and y in the presence of model imprecision on $a_1, a_2,$ and G. By using

inverse kinematics method, the control problem to track desired end-effectors spatial

trajectories $x_d(t)$, $y_d(t)$ of planar arm are equivalent to track the following joint

trajectories given by

$$\theta_2^*(t) = \cos^{-1}\frac{(x_d^2 + y_d^2 - l_1^2 - l_2^2)}{2l_1 l_2} \tag{7.13a}$$

$$\theta_1^*(t) = \tan^{-1}(\frac{y_d}{x_d}) - \tan^{-1}\left[\frac{(l_2 \sin\theta_2^*)}{(l_1 + l_2 \cos\theta_2^*)}\right] \tag{7.13b}$$

Therefore, the spatial tracking problem can be transformed into a tracking

problem for the shoulder and elbow joint angles θ_1 and θ_2. Let $\theta_1^*(t)$ and $\theta_2^*(t)$ be

smooth functions of time that represent the desired trajectories for the shoulder and

elbow joint angles.

Define two sliding surfaces $s_i, i = 1, 2$ as:

$$s_i = \dot{e}_i + \lambda_i e_i \tag{7.14}$$

where $e_i = \theta_i - \theta_i^*$ are tracking errors and λ_i are positive scalar design parameters

which control the bandwidth of the closed-loop system. Then the tracking problem

can be translated into finding inputs $[\Delta p_s, \Delta p_e]^T$ that verify the individual sliding

conditions

$$\frac{1}{2}\frac{d}{dt}s_i^2 \leq -\eta_i |s_i| \tag{7.15}$$

with $\eta_i > 0$ in the presence of parametric uncertainty.

Assume the estimations of a_1, a_2 and G are $\hat{a}_1, \hat{a}_2$ and $\hat{G}$ respectively,

which meet the following conditions:

$$\left|\hat{a}_i - a_i\right| \le A_i \tag{7.16a}$$

$$G = (I + \Delta)\hat{G} \tag{7.16b}$$

where A_i, $i = 1, 2$ are some known positive functions and Δ is a 2×2 matrix with elements Δ_{ij} satisfying $\left|\Delta_{ij}\right| \le \delta_{ij}$ for $i, j = 1, 2$, where δ_{ij} are known positive functions such that $I + \Delta$ is nonsingular. To not lose controllability, τ_{1s} and τ_{1e} must be assumed such that G is nonsingular over the entire state space and that $\hat{G}$ is invertible, continuously dependent on the parametric uncertainties and such that $\hat{G} = G$ in the absence of parametric uncertainty.

Let the sliding mode control law $U(t)$ be given by:

$$U = U_{EQ} + U_{SW} \tag{7.17}$$

where $U = [\Delta P_s, \Delta P_e]^T$, U_{EQ} is the equivalent control part, and U_{SW} is the switching control part, specified as:

$$U_{EQ} = \hat{G}^{-1}\left[\dot{\theta}_1^* - \hat{a}_1 - \lambda_1 e_1 \quad \dot{\theta}_2^* - \hat{a}_2 - \lambda_2 e_2\right]^T \tag{7.18a}$$

$$U_{SW} = \hat{G}^{-1}\left[k_1 \mathrm{sat}\left(\frac{s_1}{\Phi_1}\right) \quad k_2 \mathrm{sat}\left(\frac{s_2}{\Phi_2}\right)\right]^T \tag{7.18b}$$

where

$$\mathrm{sat}(y) = \begin{cases} y, & |y| \le 1 \\ \mathrm{sgn}(y), & \text{otherwise} \end{cases} \tag{7.19}$$

In addition, Φ_i, $i = 1, 2$ are the boundary layer thicknesses, k_1 and k_2 are positive

constants.

Since

$$\dot{s}_1 = \hat{a}_1 - a_1 + \Delta_{11}(\dot{\theta}_1^* - \lambda e_1 - \hat{a}_1) + \Delta_{12}(\dot{\theta}_1^* - \lambda e_1 - \hat{a}_2)$$
$$- \Delta_{12}k_2 \operatorname{sgn}(s_2) - (1 + \Delta_{11})k_1 \operatorname{sgn}(s_1) \tag{7.20a}$$

$$\dot{s}_2 = \hat{a}_2 - a_2 + \Delta_{21}(\dot{\theta}_2^* - \lambda e_2 - \hat{a}_1) + \Delta_{22}(\dot{\theta}_2^* - \lambda e_2 - \hat{a}_2)$$
$$- \Delta_{21}k_1 \operatorname{sgn}(s_1) - (1 + \Delta_{22})k_2 \operatorname{sgn}(s_2) \tag{7.20b}$$

the sliding conditions (7.15) are verified if

$$(1 - \delta_{11})k_1 \geq A_1 + \delta_{11}\left|\dot{\theta}_1^* - \lambda_1 e_1 - \hat{a}_1\right| + \delta_{12}\left|\dot{\theta}_1^* - \lambda_1 e_1 - \hat{a}_2\right| - \delta_{12}k_2 \tag{7.21a}$$

$$(1 - \delta_{22})k_1 \geq A_2 + \delta_{21}\left|\dot{\theta}_2^* - \lambda_2 e_2 - \hat{a}_1\right| + \delta_{22}\left|\dot{\theta}_2^* - \lambda_2 e_2 - \hat{a}_2\right| - \delta_{21}k_1 \tag{7.21b}$$

and, particularly, k_1 and k_2 are chosen such that

$$(1 - \delta_{11})k_1 + \delta_{12}k_2 = A_1 + \delta_{11}\left|\dot{\theta}_1^* - \lambda_1 e_1 - \hat{a}_1\right| + \delta_{12}\left|\dot{\theta}_1^* - \lambda_1 e_1 - \hat{a}_2\right| + \eta_1 \tag{7.22a}$$

$$(1 - \delta_{22})k_1 + \delta_{21}k_1 = A_2 + \delta_{21}\left|\dot{\theta}_2^* - \lambda_2 e_2 - \hat{a}_1\right| + \delta_{22}\left|\dot{\theta}_2^* - \lambda_2 e_2 - \hat{a}_2\right| + \eta_2 \tag{7.22b}$$

It is well-known that the Frobenius-Perron theorem guarantees that (7.22a) and (7.22b) have a unique nonnegative solution $[k_1, k_2]$. Therefore, the control law (7.17) with k_1, k_2 defined by (7.22) meets the sliding conditions (7.15) in the presence of parametric uncertainties bounded as in (7.16).

Therefore, when the state trajectories are outside their respective boundary layers, since the control law guarantees that the boundary layers are attractive; the trajectories approach the boundary layers and reach them in finite times. Once inside the boundary layers, the state trajectories remain inside them for all later time and approach neighborhoods of $e_i = 0$ asymptotically.

Taking the Laplace transform of e_i gives

$$e_i = \frac{1}{s + \lambda_i} s_i \tag{7.23}$$

Then, since $|s_i| \leq \Phi_i, \forall t \geq t_1$ with t_1 finite, it is easy to show

$$\lim_{t_0 \to \infty} \sup_{t \geq t_0} |\theta_i - \theta_i^*| \leq \frac{\Phi_i}{\lambda_i} \tag{7.24}$$

Thus, the tracking error eventually enters neighborhoods of $e_i = 0$, the sizes of which are inversely proportional to λ_i. Therefore, if λ_i is larger, tracking errors are smaller.

In practical systems, however, the constraint of the actuators, typically as structural resonant modes, neglected time delays, and sampling rates tend to limit the control bandwidths λ_i. The desired control bandwidth is the minimum of those three bounds [21]. In addition, if the control bandwidth is chosen to be very large, it will excite the high-frequency unmodeled dynamics; hence the likelihood of chattering increases. For these reasons, the control bandwidth cannot be increased arbitrarily and should be kept within some reasonable range.

In order to improve tracking performance while avoiding chattering under physical limitations, effort is made to improve the sliding mode controller via fuzzy logic. In this work, individual Mamdani fuzzy systems are used to adjust control bandwidths λ_i based on the corresponding tracking errors.

The basic design philosophy of the controller is that when tracking errors are far from the origin, the control bandwidths λ_i are designed to be large so that the

error trajectories eventually enter small neighborhoods of zero (7.24). As this small neighborhood is approached (i.e. tracking errors are small), the control bandwidths λ_i are reduced to avoid chattering. The time-varying control bandwidths λ_i are determined by using the fuzzy systems based on tracking errors, which makes the sliding surfaces time varying.

The fuzzy system rule base for control bandwidths λ_i is defined as follows:

$$
\begin{aligned}
&\text{Rule 1}: \quad \text{IF } e_i \in R_i^1 \text{ THEN } \lambda_i = \lambda_i^1, \\
&\text{Rule 2}: \quad \text{IF } e_i \in R_i^2 \text{ THEN } \lambda_i = \lambda_i^2, \\
&\qquad\qquad \vdots \\
&\text{Rule } j: \quad \text{IF } e_i \in R_i^j \text{ THEN } \lambda_i = \lambda_i^j, \, j = 1, ..., r_i
\end{aligned}
\tag{7.25}
$$

where e_i is the tracking error for the ith system variable, and r_i is the total number of rules for the ith system variable. In (7.25), R_i^j is the jth fuzzy set on the ith universe of discourse, characterized by membership function $\mu_i^j(e_i)$.

Therefore, for each tracking error e_i, a fuzzy system is built such that each rule j has a specific control bandwidth in the consequent part. The aggregate control bandwidth λ_{i_f} is obtained by center average defuzzification and can be viewed as a nonlinear interpolation between linear mappings:

$$
\lambda_{i\_f} = \frac{\sum_{j=1}^{r_i} \mu_i^j \lambda_i^j}{\sum_{j=1}^{r_i} \mu_i^j}
\tag{7.26}
$$

Based on the result from (7.26), the resulting sliding surface is represented as:

$$
s_{i\_f} = \dot{e}_i + \lambda_{i\_f} e_i
\tag{7.27}
$$

Finally, the proposed fuzzy sliding mode control law is:

$$
U = U_{EQ} + U_{SW\_f}
\tag{7.28}
$$

where $U = \left[\Delta P_s, \ \Delta P_e \right]^T$ and

$$U_{EQ} = \hat{G}^{-1} \left[\dot{\theta}_1^* - \hat{a}_1 - \lambda_1 e_1 \quad \dot{\theta}_2^* - \hat{a}_2 - \lambda_2 e_2 \right]^T \qquad (7.29a)$$

$$U_{SW\_f} = \hat{G}^{-1} \left[k_1 \text{sat}\left(\frac{s_{1\_f}}{\Phi_1} \right) \quad k_2 \text{sat}\left(\frac{s_{2\_f}}{\Phi_2} \right) \right]^T \qquad (7.29b)$$

7.3   SIMULATION RESULTS

The planar arm actuated by four groups of PMs given by (7.12) is simulated using a 4th-order Runge-Kutta algorithm with step size of 0.01 second.   For the simulations, all the physical quantities of the manipulator (i.e. lengths, masses, etc.) are assumed to be exactly known and listed in Table 2.

Table 2   Physical Parameters for Planar Arm.

PM Units	Length of Links	Mass of Links	Radius of Pulleys	Number of muscle pairs
Shoulder	0.46 m	10 kg	7.62 cm	6
Elbow	0.46 m	10 kg	5.08 cm	3

The PM coefficients i.e. $F, K,$ and B are assumed to be not known with precision.   Assume all shoulder PMs are matched to each other, but not to the elbow PMs.   Similarly, all elbow PMs are assumed to be matched to each other, but not to the shoulder PMs.

The fuzzy sliding mode control is designed based on (7.26)-(7.29).   In the simulation, two identical three-rule fuzzy systems are used to adjust each control bandwidth, although each fuzzy system can be different generally.

The fuzzy system is given by

Rule 1: IF $e_i \in R^1$ THEN $\lambda_i = \lambda_i^1$

Rule 2: IF $e_i \in R^2$ THEN $\lambda_i = \lambda_i^2$ $i = 1, 2$ (7.30)

Rule 3: IF $e_i \in R^3$ THEN $\lambda_i = \lambda_i^3$

The fuzzy sets R^1, R^2, and R^3 are characterized by the membership functions shown in Figure 15 where

$$d_1 = -0.01, \quad d_2 = -0.005, \quad d_3 = 0.005, \quad d_4 = 0.01 \tag{7.31}$$
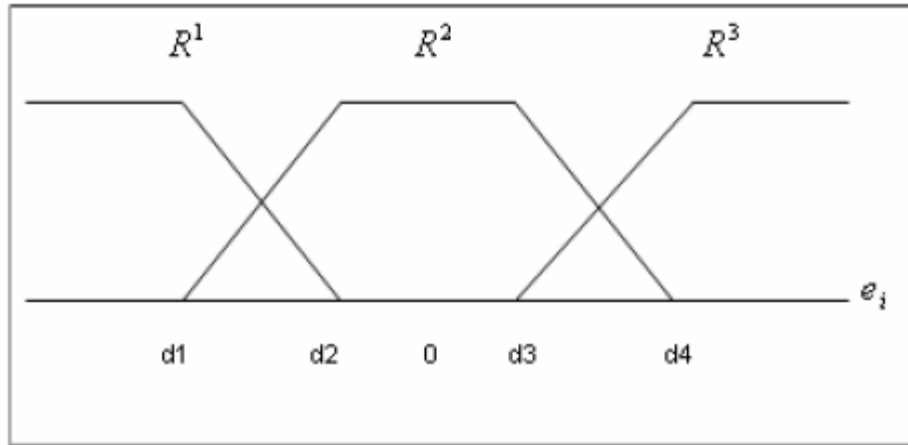

Figure 15 - Input membership functions of the fuzzy system

The consequent parts of both systems are characterized as

$$\lambda_i^1 = 25, \ \lambda_i^2 = 5, \ \lambda_i^3 = 25, \ i = 1, 2 \tag{7.32}$$

Accordingly, the individual control bandwidths are given by:

$$\lambda_{i\_f} = \frac{\sum_{j=1}^{3} \mu_i^j \lambda_i^j}{\sum_{j=1}^{3} \lambda_i^j}, \ i = 1, 2 \tag{7.33}$$

where $\mu_i^j, i = 1, 2$ are shown in Figure 15.

The resulting time-varying sliding surfaces are obtained by:

$$s_{i\_f} = \dot{e}_i + \lambda_{i\_f} e_i \tag{7.34}$$

The idea of this controller is for the sliding surface to have a larger slope λ when the tracking error is larger, and to decrease the slope as the error decreases. The larger slope results in smaller steady-state tracking error being achieved initially, and the reduced slope results in less chattering once tracking has been achieved, hence more accurate steady-state tracking.

To investigate the robustness of the sliding mode controller, $F, K,$ and B coefficients (i.e. K_0, K_1, etc.) are randomly chosen from a uniform distribution within $\pm 50\%$ of their nominal values. Hence, $A_1 = 25$ and $A_2 = 15.0$ are chosen to satisfy (7.16). We also have $\Delta = \left[\Delta_{ij}\right]$ where

$$\left|\Delta_{ij}\right| \le \delta_{ij} = \begin{cases} 0.5, & i = j \\ 0, & i \ne j \end{cases} \tag{7.35}$$

The control gains are chosen as $k_i = 50, \ i = 1, 2$ to meet (7.22). In the simulation, initial conditions are $\theta_1(0) = -\dfrac{\pi}{4}$, $\theta_2(0) = \dfrac{\pi}{2}$, $P_{0bs} = P_{0te} = 310.3\,\text{kPa}$, $P_{0ts} = 449.6\,\text{kPa}$ and $P_{0be} = 310.5\,\text{kPa}$. These nominal pressures are chosen so that (a) the PM pressures remain within the permissible range of $206.8 - 620.5$ kPa (30 - 90 psi) for this type of PM throughout the control mission, and (b) in the absence of control, the shoulder and elbow angles revert to $\theta_1 = -\dfrac{\pi}{4}$, $\theta_2 = \dfrac{\pi}{2}$.

Three kinds of basic tracking tasks for the end effector are investigated: a

vertical line, a sinusoidal spline and a circle.   These spatial paths can be converted to equivalent joint angle trajectories via inverse kinematics of the two-joint planar arm. The performance of the FSMC controller is compared with that of a traditional SMC applied to the same plant.   For a meaningful comparison between the proposed FSMC and the traditional SMC, both control methods are applied to identical physical systems, i.e. all the physical quantities of the manipulator are those in Table 2 and the PM coefficients are the same.   Incidentally, the PM coefficient sets used were chosen from many sets randomly generated from a uniform distribution within $\pm 50\%$ of their assumed values.   Only those sets producing the largest errors were used in the simulations, so that the robustness of the method could be investigated via simulation.

Vertical line:

The *x* and *y* components of the desired spatial path for the end effector to follow are given by:

$$
\begin{aligned}
x_d(t) &= 0.6096 \\
y_d(t) &= 0.39624 + 0.24384\sin(0.4\pi t - \frac{\pi}{2})
\end{aligned}
\tag{7.36}
$$

The joint angle tracking results using traditional sliding mode control are shown in Figure 16, and joint angle tracking errors with the proposed fuzzy sliding mode control are shown in Figure 17.

Comparing these two figures, the better tracking performance is achieved in Figure 17, i.e. the proposed FSMC, without obvious chattering.   Both joint angle tracking errors with FSMC are kept within 0.01 rad., which is better than 0.035 rad. for the elbow joint and 0.06 rad. for the shoulder joint in SMC.

Figure 16 - Joint angle tracking errors (vertical line, SMC).

Inset – spatial performance.

Figure 17 - Joint angle tracking errors (vertical line, FSMC).

Sinusoidal spline:

The desired spatial path for the sinusoidal spline is given by:

$$x_d(t) = 0.1524 + 0.1219t$$
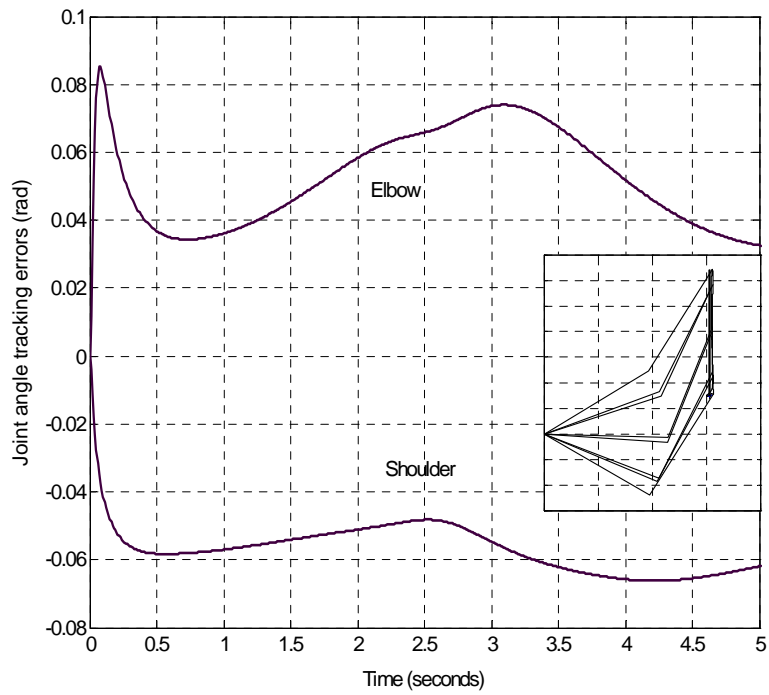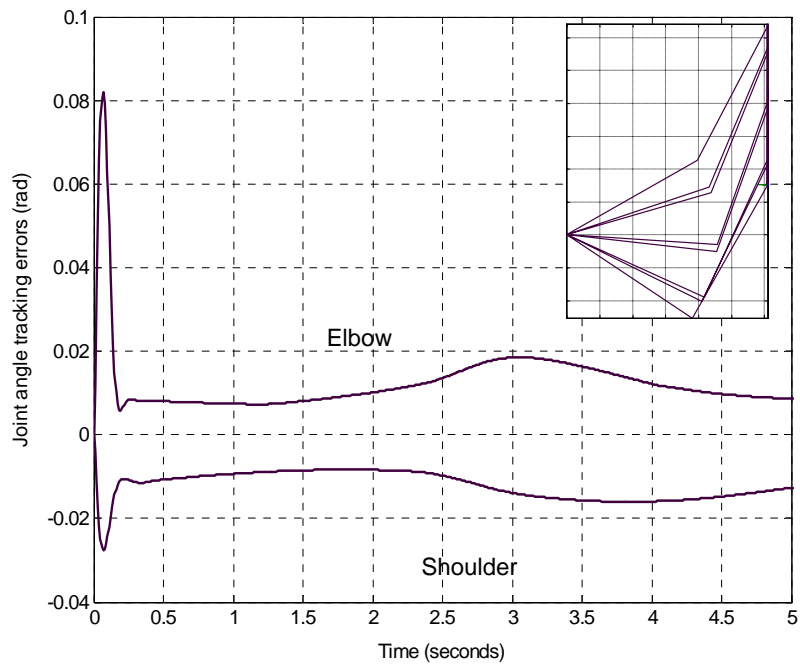$$y_d(t) = 0.39624 + 0.24384 \sin\left(0.4\pi t - \frac{\pi}{2}\right) \tag{7.37}$$

Figure 18 - Joint angle tracking errors (spline, SMC).

Inset – spatial performance
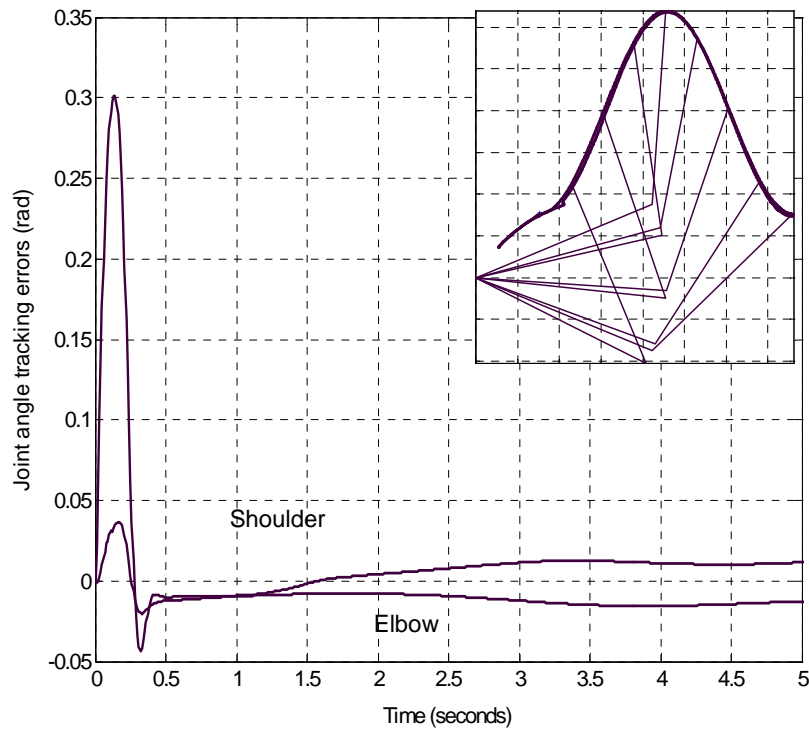
Figure 19 - Joint angle tracking errors (spline, FSMC).

Inset – spatial performance.

The joint angle tracking errors with traditional SMC are shown in Figure 18, and the results from fuzzy sliding mode control are shown in Figure 19. Obviously, the better tracking performance is obtained by the proposed FSMC.

Circle:

The desired spatial path for the circle is given by:

$$x_d(t) = 0.36576 + 0.3048 \sin(0.4\pi t - 0.7754)$$
$$y_d(t) = 0.36576 + 0.3048 \cos(0.4\pi t + 2.3462)$$

$$(7.38)$$

The joint angle tracking error with the traditional SMC is shown in Figure 20, and the results from fuzzy sliding mode control are shown in Figure 21. Compared with SMC, FMSC provides much better tracking performance with no obvious chattering.
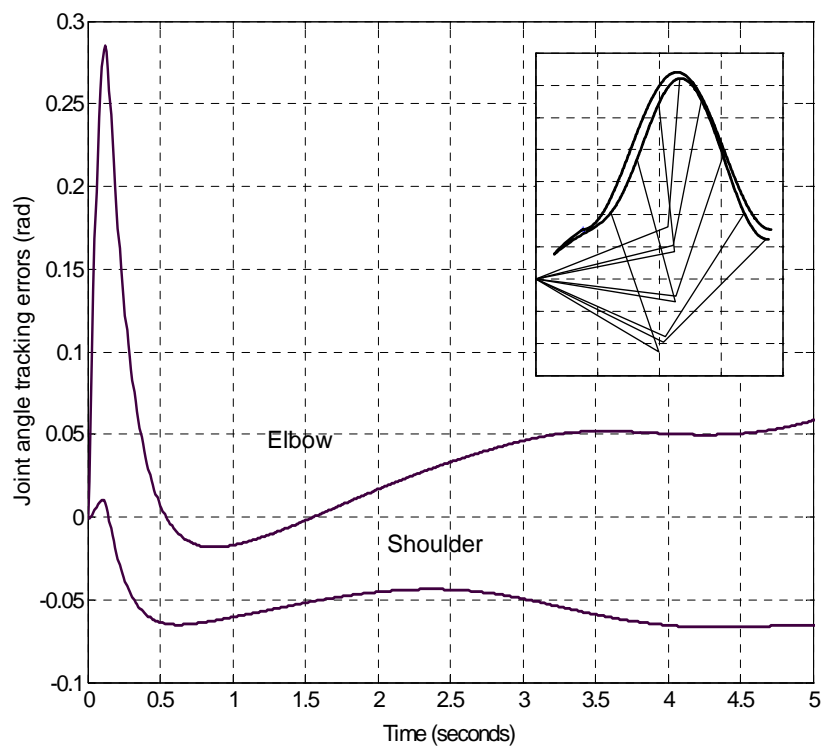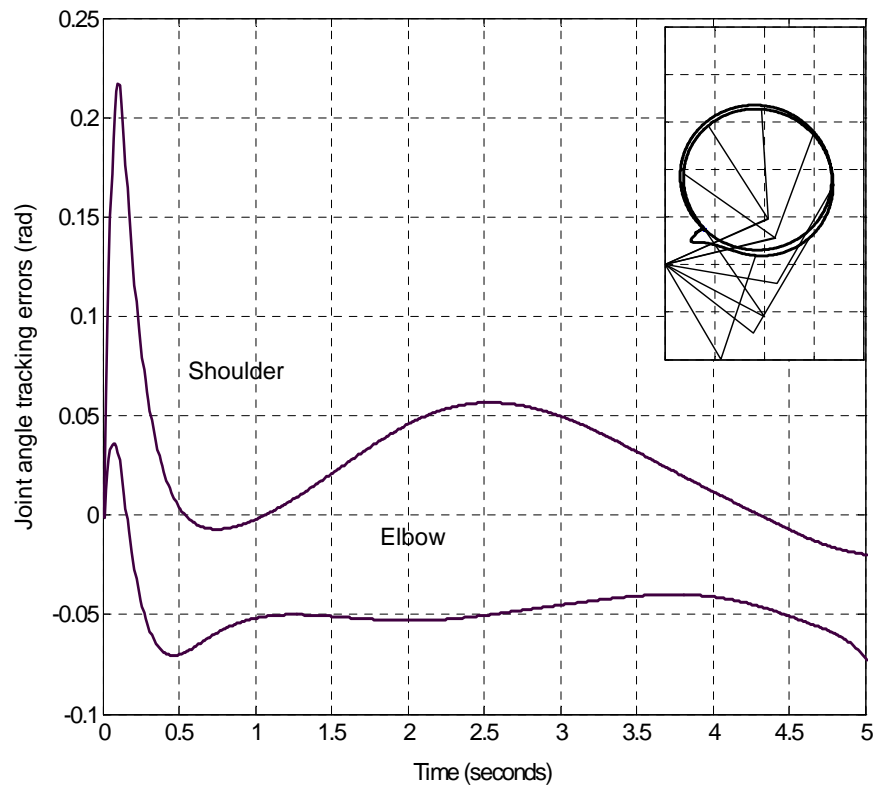
Figure 20 - Joint angle tracking errors (circle, SMC).

Inset – spatial performance
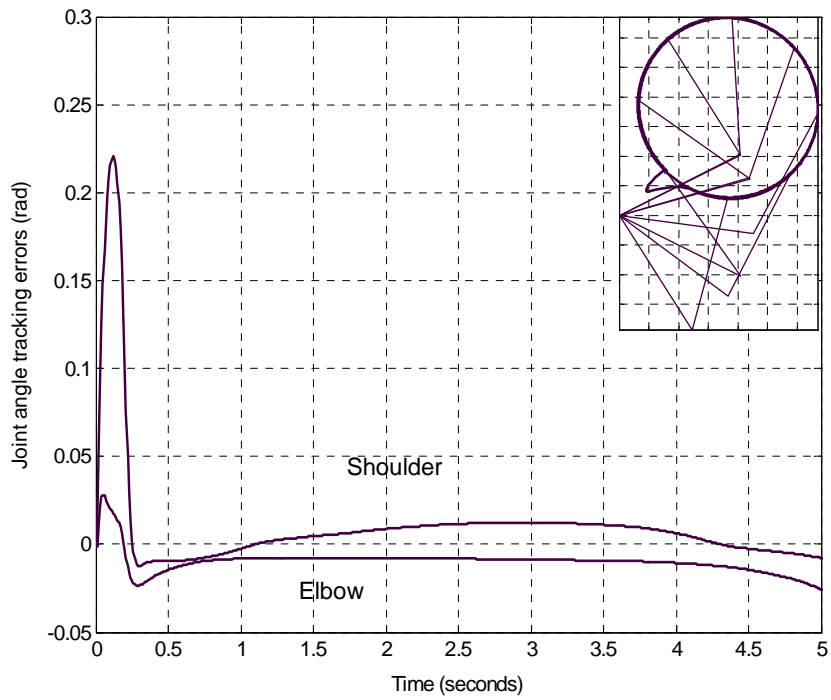
Figure 21 - Joint angle tracking errors (circle, FSMC).
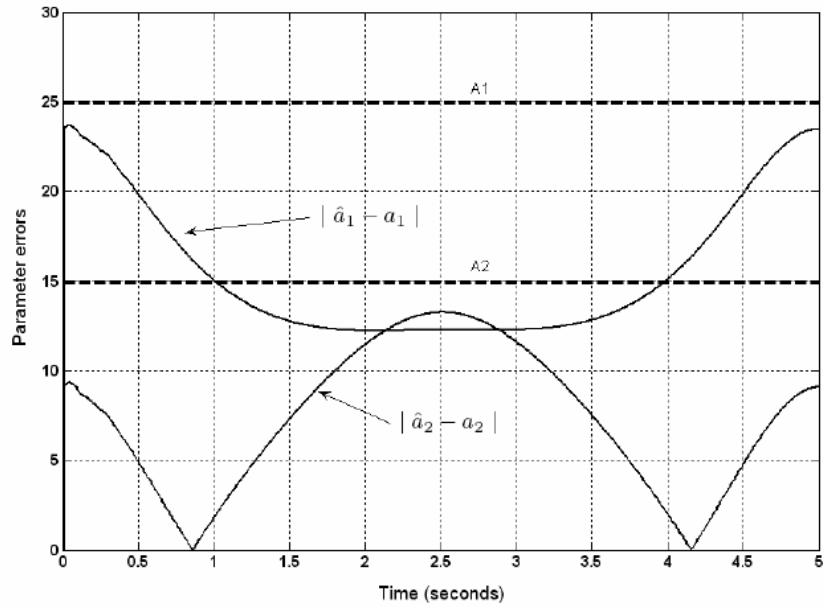
Figure 22 - Comparison of $|\hat{a}_i - a_i|$ with their nominal range(circle, FSMC)
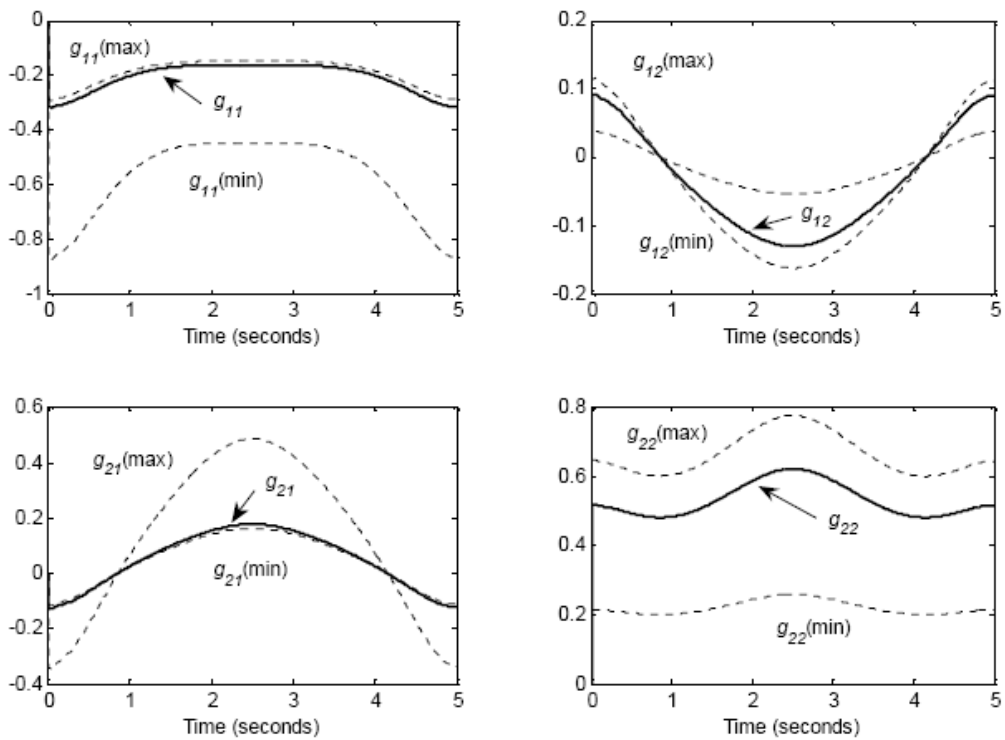
Figure 23 - Individual elements of G with their nominal ranges (Circle, FSMC)

In addition to the above, the parameter errors for the controller are plotted. Figure 22 shows the relationship between system parameters $a_i, i = 1, 2$ and their

estimated values $\hat{a}_i$. From Figure 21, it is seen that $|\hat{a}_1 - a_1|$ is always less than $A_1 = 25$, and $|\hat{a}_2 - a_2|$ is always less than $A_1 = 15$, as dictated by (7.16a). Figure 23 shows the relationship between the elements of G and their theoretical ranges. Close inspection of the bounds of Figure 22 (especially g_{12} and g_{21}) reveals that the actual values of each element do remain within their estimated upper and lower bounds, satisfying (7.16b).

7.4 DISCUSSION

The tracking performance acquired by the control of fuzzy sliding mode is seen to be superior to those with traditional sliding mode control. This is because the control bandwidth of fuzzy sliding mode is designed to be relatively larger when the tracking trajectory is far from the desired, and designed to be relative smaller when the tracking error comes within a neighborhood of zero. The smooth transition in control bandwidth is realized via the fuzzy system. The adjustable control bandwidth leads to smaller tracking error in the vicinity of the desired trajectory. Since the analysis made here is on the basis of assumption that only one type of PM exists in the system, it may not accurately describe the behavior of systems using other types of PMs. Various constructions of PMs may include different types of rubber or plastic, different sheathing, different sizes of PM, and different pressure valves, among other things. All these factors affect the PM coefficients *F*, *K*, and *B*. In addition, some PM constructions may not admit a spring/damper/contractile element model at all. In such cases, the PM may have to be modeled from scratch.

Nevertheless, there are always inaccuracies associated with any simulation. One source of error in the case of PMs stems from the fact that PMs are quite heat sensitive. PM coefficients are known to vary significantly with temperature, and PM

temperature varies with use, due to friction.   Therefore, these results cannot be taken as accurate with extended PM use.   Change of PM characteristics was not taken into account in these simulations.

There is no general agreement among researchers as to the effects of heating on PMs.   Another source of inaccuracy is the fact that the PMs will not be perfectly matched, as assumed in the paper.   This would imply they are all constructed identically to each other, with identical dimensions, materials, etc.   Consideration of unmatched PMs is beyond the scope of this research.

CHAPTER VIII

INTEGRAL SLIDING MODE TRACKING CONTROL
OF A TWO-JOINT MANIPULATOR ACTUATED BY FOUR PM GROUPS

8.1 INTEGRAL SLIDING MODE CONTROL OF A TWO-JOINT MANIPULATOR MODEL

Regarding the two-joint planar arm model mentioned in the previous chapter, we know it is difficult to have perfect knowledge of coefficients $F, K,$ and B for all PMs due to the nonlinear, time-varying characteristics of PMs. In practice, the PM may also suffer some external disturbance such as static and Coulomb friction. An additional term describing the effect of noise hence needs to be introduced into the system model.

Therefore, the system model of two-joint planar arm should be presented as:

$$\ddot{\theta} = A + GU + N \tag{8.1}$$

where

$$\ddot{\theta} = \begin{bmatrix} \ddot{\theta}_1 \\ \ddot{\theta}_2 \end{bmatrix} \qquad U = \begin{bmatrix} \Delta P_s \\ \Delta P_e \end{bmatrix} \qquad N = \begin{bmatrix} n_1 \\ n_2 \end{bmatrix} \tag{8.2}$$

and N is a 2×1 matrix, which represents external perturbations.

Again, the estimations of a_1, a_2, G are assumed, which are $\hat{a}_1, \hat{a}_2, \hat{G}$, respectively, meeting the conditions:

$$\left| \hat{a}_i - a_i \right| \le A_i \tag{8.3a}$$

$$G = (I + \Delta)\hat{G} \tag{8.3b}$$

where $A_i, i = 1, 2$ are some known positive functions of $(\theta_1, \dot{\theta}_1, \theta_2, \dot{\theta}_2)$ and

Δ is a 2×2 matrix with elements Δ_{ij} satisfying $|\Delta_{ij}| \leq \delta_{ij}$ $i, j = 1, 2$.

Assume the ith element of N is bounded by a known upper bound B_i:

$$|n_i| \leq B_i, i = 1, 2 \tag{8.4}$$

In (8.1), both the parametric uncertainties i.e. imprecision on a_1, a_2, G and the external disturbance result in inaccuracies of the model parameters. The control problem is to determine the input functions $\Delta P_s(t)$ and $\Delta P_e(t)$ to force the end effector E to follow a desired path in the spatial variables x and y in the presence of both model imprecision on a_1, a_2, G and external disturbances.

By using the inverse kinematics of the planar arm, the spatial tracking problem can be transformed into a tracking problem for the shoulder and elbow joint angles θ_1 and θ_2. Let $\theta_1^*(t)$ and $\theta_2^*(t)$ be smooth functions of time that represent the desired trajectories for the shoulder and elbow joint angles. Define two integral sliding surfaces $s_i, i = 1, 2$ as:

$$s_i = s_{Ti} + s_{Ii} \tag{8.5}$$

where s_{Ti} are traditional sliding surface parts and s_{Ii} are integral parts.
Define

$$s_{Ti} = \dot{e}_i + \lambda_{1i} e_i \tag{8.6}$$

where $e_i = \theta_i - \theta_i^*$ are tracking errors and λ_{1i} are positive scalar design parameters. Define

$$s_{Ii} = \lambda_{2i} \int_0^t e_i(\tau)d\tau - \lambda_{1i}e_i(0) - \dot{e}_i(0) \qquad (8.7)$$

where λ_{2i} are positive scalar design parameters.

If the individual sliding modes could be enforced by a properly designed input, then $\dot{s}_i = 0$ as well [39, 42]. From (8.7), this leads to

$$\ddot{e}_i + \lambda_{1i}\dot{e}_i + \lambda_{2i}e_i = 0 \qquad (8.8)$$

This represents the ideal error dynamics, independently of system uncertainties and external perturbations. Hence, the integral sliding surface determines the desired error dynamics to have an ideal second order dynamics in each link.

The control law $U(t)$ is given by:

$$U = U_{EQ} + U_{SW} \qquad (8.9)$$

where $U = [\Delta P_s, \Delta P_e]^T$, U_{EQ} is the equivalent control, and U_{SW} is the switching control. The function of U_{EQ} is to maintain the trajectory on the sliding surface, and the function of U_{SW} is to guide the trajectory to this surface.

Let the sliding surface vector be given by:

$$S = [s_1 \quad s_2]^T \qquad (8.10)$$

Differentiating (8.10) gives:

$$\dot{S} = \begin{bmatrix} \ddot{e}_1 + \lambda_{11}\dot{e}_1 + \lambda_{21}e_1 \\ \ddot{e}_2 + \lambda_{12}\dot{e}_2 + \lambda_{22}e_2 \end{bmatrix} \tag{8.11}$$

First, consider the model (8.1) without external perturbation, i.e. (7.12). Substituting (7.12) into (8.11) gives:

$$\dot{S} = A + GU - \begin{bmatrix} -\ddot{\theta}_1^* + \lambda_{11}\dot{e}_1 + \lambda_{21}e_1 \\ -\ddot{\theta}_2^* + \lambda_{12}\dot{e}_2 + \lambda_{22}e_2 \end{bmatrix} \tag{8.12}$$

The equivalent control U_{EQ} is obtained by equating (8.12) to zero:

$$U_{EQ} = \hat{G}^{-1}\left(\begin{bmatrix} \ddot{\theta}_1^* \\ \ddot{\theta}_2^* \end{bmatrix} - \begin{bmatrix} \lambda_{11} & 0 \\ 0 & \lambda_{12} \end{bmatrix}\begin{bmatrix} \dot{e}_1 \\ \dot{e}_2 \end{bmatrix} - \begin{bmatrix} \lambda_{21} & 0 \\ 0 & \lambda_{22} \end{bmatrix}\begin{bmatrix} e_1 \\ e_2 \end{bmatrix}\right) - \hat{G}^{-1}\begin{bmatrix} \hat{a}_1 \\ \hat{a}_2 \end{bmatrix} \tag{8.13}$$

The switching control U_{SW} is given by:

$$U_{SW} = \begin{bmatrix} u_{sw1} \\ u_{sw2} \end{bmatrix} = -K\begin{bmatrix} \mathrm{sgn}(s_1) \\ \mathrm{sgn}(s_2) \end{bmatrix} \tag{8.14}$$

where K is a 2×2 positive definite diagonal matrix with its ith diagonal element satisfying $k_i > B_i, i = 1, 2$.

Since U_{SW} is essentially a high frequency discontinuous sign function, to alleviate chattering in practical implementations, a continuous approximation of U_{SW} is used. From [39, 42], the continuous approximation value $U_{SW}^{'}$ is equal to the average value measured by a first order linear filter with U_{SW} as its input. The following equation is hence obtained:

74

$$\Gamma \dot{U}_{SW}^{'} + U_{SW}^{'} = U_{SW} \qquad (8.15)$$

where

$$U_{SW}^{'} = \begin{bmatrix} u_{sw1}^{'} \\ u_{sw2}^{'} \end{bmatrix} \qquad (8.16a)$$

$$\Gamma = \begin{bmatrix} \tau_1 & 0 \\ 0 & \tau_2 \end{bmatrix} \qquad (8.16b)$$

and τ_i, $i = 1, 2$ are the time constants.

Transforming (8.15) into the time domain, we can easily reach that:

$$u_{sw1}^{'} = (1/\tau_1)e^{-(1/\tau_1)t}u_{sw1} \qquad (8.17a)$$

$$u_{sw2}^{'} = (1/\tau_2)e^{-(1/\tau_2)t}u_{sw2} \qquad (8.17b)$$

Finally, the proposed integral sliding mode control law is presented as:

$$U = U_{EQ} + U_{SW}^{'} \qquad (8.18)$$

Since

$$\begin{aligned} s_1 = \hat{a}_1 - a_1 &+ \Delta_{11}(\ddot{\theta}_1^{*} - \lambda_{11}\dot{e}_1 - \lambda_{21}e_1 - \hat{a}_1) + \Delta_{12}(\ddot{\theta}_1^{*} - \lambda_{11}\dot{e}_1 \\ &- \lambda_{21}e_1 - \hat{a}_2) - \Delta_{12}k_2\,\mathrm{sgn}(s_2) - (1 + \Delta_{11})k_1\,\mathrm{sgn}(s_1) \end{aligned} \qquad (8.19a)$$

$$\begin{aligned} s_2 = \hat{a}_2 - a_2 &+ \Delta_{21}(\ddot{\theta}_2^{*} - \lambda_{12}\dot{e}_2 - \lambda_{22}e_2 - \hat{a}_1) + \Delta_{22}(\ddot{\theta}_2^{*} - \lambda_{12}\dot{e}_2 \\ &- \lambda_{22}e_2 - \hat{a}_2) - \Delta_{21}k_1\,\mathrm{sgn}(s_1) - (1 + \Delta_{22})k_2\,\mathrm{sgn}(s_2) \end{aligned} \qquad (8.19b)$$

the individual sliding conditions

$$\frac{1}{2}\frac{d}{dt}s_i^2 \le -\eta|s_i| \qquad (8.20)$$

are satisfied if there exist constants k_1 and k_2 such that

$$(1-\delta_{11})k_1 \geq A_1 + \delta_{11}\left|\ddot{\theta}_1^* - \lambda_{11}\dot{e}_1 - \lambda_{21}e_1 - \hat{a}_1\right| +$$
$$\delta_{12}\left|\ddot{\theta}_1^* - \lambda_{11}\dot{e}_1 - \lambda_{21}e_1 - \hat{a}_2\right| - \delta_{12}k_2 \tag{8.21a}$$

$$(1-\delta_{22})k_2 \geq A_2 + \delta_{21}\left|\ddot{\theta}_2^* - \lambda_{12}\dot{e}_2 - \lambda_{22}e_2 - \hat{a}_1\right| +$$
$$\delta_{22}\left|\ddot{\theta}_2^* - \lambda_{12}\dot{e}_2 - \lambda_{22}e_2 - \hat{a}_2\right| - \delta_{21}k_1 \tag{8.21b}$$

In particular, let k_1 and k_2 be chosen such that

$$(1-\delta_{11})k_1 = A_1 + \delta_{11}\left|\ddot{\theta}_1^* - \lambda_{11}\dot{e}_1 - \lambda_{21}e_1 - \hat{a}_1\right| +$$
$$\delta_{12}\left|\ddot{\theta}_1^* - \lambda_{11}\dot{e}_1 - \lambda_{21}e_1 - \hat{a}_2\right| - \delta_{12}k_2 \tag{8.22a}$$

$$(1-\delta_{22})k_2 = A_2 + \delta_{21}\left|\ddot{\theta}_2^* - \lambda_{12}\dot{e}_2 - \lambda_{22}e_2 - \hat{a}_1\right| +$$
$$\delta_{22}\left|\ddot{\theta}_2^* - \lambda_{12}\dot{e}_2 - \lambda_{22}e_2 - \hat{a}_2\right| - \delta_{21}k_1 \tag{8.22b}$$

The Frobenius–Perron theorem guarantees that (8.22a) and (8.22b) have a unique nonnegative solution $[k_1, k_2]$. Therefore, the control law (8.18) with such $[k_1, k_2]$ verifies the sliding conditions in the presence of both parametric uncertainties bounded as in (8.3a) and external perturbation bounded as in (8.3b).

Therefore, the control law (8.18) drives the state trajectory of the PM model onto the sliding surface in the presence of model uncertainties and external perturbations. Once on the surface, the system trajectory remains a neighborhood of the desired trajectory for all subsequent time. Thus, satisfying the sliding condition makes the surface an invariant set, i.e. a set for which any trajectory starting from an initial condition within the set remains in the set for all future time.

8.2 SIMULATION RESULTS

The planar robot arm actuated by PMs given by (8.1) and (8.18) is simulated using a 4th-order Runge-Kutta algorithm with step size of 0.01 second. All the physical quantities (length, mass, etc) of shoulder and elbow links are assumed to be exactly known as stated before, which are listed in Table 2. Again, without losing generality, all shoulder PMs are assumed to be identical to each other (i.e. all physical quantities for each shoulder PM are the same), but not to the elbow PMs. Similarly, all elbow PMs are assumed to be matched to each other, but not to the shoulder PMs. The coefficients $F, K,$ and B are assumed to be not known precisely, hence the nominal values vary to some extent. In this case, the actual values are assumed to be within 50 percent of their nominal values.

The nominal PMs coefficients for planar arm and their actual values used for the simulation [57] are listed in Table 3:

Table 3   Coefficients for PMs

Coefficients	Nominal values	Actual values	
		Elbow	Shoulder
F_0	1.79e+2	2.58e+2	1.53e+2
F_1	1.39	1.67	0.763
K_0	5.71	7.70	7.17
K_1	3.07e-2	2.18e-2	4.28e-2
B_{0i}	1.01	0.965	0.794
B_{1i}	6.91e-3	4.02e-3	5.19e-3
B_{0d}	6e-1	8.11e-1	8.60e-1
B_{1d}	-8.03e-4	-8.53e-4	-5.07

To investigate robustness, only those coefficient sets producing the largest errors were

chosen from a uniform distribution within 50 percent of their assumed values.

Based on the quantities above, the quantities $A_1 = 12.5$ and $A_2 = 15.0$ are chosen to satisfy (8.3). $\Delta = \lfloor \Delta_{ij} \rfloor$ is defined as

$$\left| \Delta_{ij} \right| \le \delta_{ij} = \begin{cases} 0.5, & i = j \\ 0, & i \ne j \end{cases} \tag{8.23}$$

The control gains are calculated as $k_i = 50, \ i = 1, 2$ to meet (8.22). Initial conditions: $\theta_1(0) = -\dfrac{\pi}{4}$, $\theta_2(0) = \dfrac{\pi}{2}$, $P_{0bs} = 310.3\,\text{kpa}$, $P_{0te} = 310.3\,\text{kpa}$, $P_{0ts} = 449.6\,\text{kpa}$, $P_{0be} = 310.5\,\text{kpa}$ are used in the simulation.

These default parameters are designed to guarantee that the PM pressures remain within the permissible range 206.8-620.5 kpa throughout the control mission and revert the shoulder and elbow angles to $\theta_1 = -\dfrac{\pi}{4}$, $\theta_2 = \dfrac{\pi}{2}$ in case of absence of control. In addition, the scalar design parameters in (8.5) are preset to $\lambda_{1i} = 40, \lambda_{2i} = 400, i = 1, 2$ and the time constants in (8.17) are $\tau_i = 0.01, i = 1, 2$ (these values for shoulder and elbow could be different though).

Three basic trajectories for the end effector are investigated in the simulation: a sinusoidal spline a sloping line, and a circle. These spatial paths can be combined together to mimic more complicated human movements. The spatial trajectories of the end effector can be converted to equivalent joint angle trajectories by the inverse kinematics of the planar robot arm.

The performance of the proposed ISMC controller is compared to that of a traditional sliding mode controller. The identical planar arm model is being investigated by both methods in order to make a meaningful comparison, i.e. both

controllers choose the same physical quantities of the model and the same coefficients of $F, K,$ and B. In addition, the PM model is designed to be interfered with external perturbation. Since Gaussian white noise is a good approximation of many external perturbations from real world, different intensities of Gaussian white noise are applied in the simulation to investigate the robustness of control performance.

Sinusoidal spline

First, a sinusoidal spline as desired for the end effector desired path is considered, with x and y coordinates given by:

$$
\begin{aligned}
x_d &= 0.1524 + 0.1219\,t \\
y_d &= 0.39624 + 0.24384\sin(0.4\pi\,t - \frac{\pi}{2})
\end{aligned}
\tag{8.24}
$$

As mentioned above, the PM model uses the parameters listed in Tables 2 and 3. In this case, Gaussian white noise is specified with the intensity of 10 dbw.

The equivalent joint angle tracking error (absolute value) using SMC is shown in Figure 24, and corresponding joint angle tracking results with ISMC are shown in Figures 25 and 26. By comparison, the tracking performance in Figures 25 and 26, i.e. the proposed ISMC is seen to be superior to basic SMC.
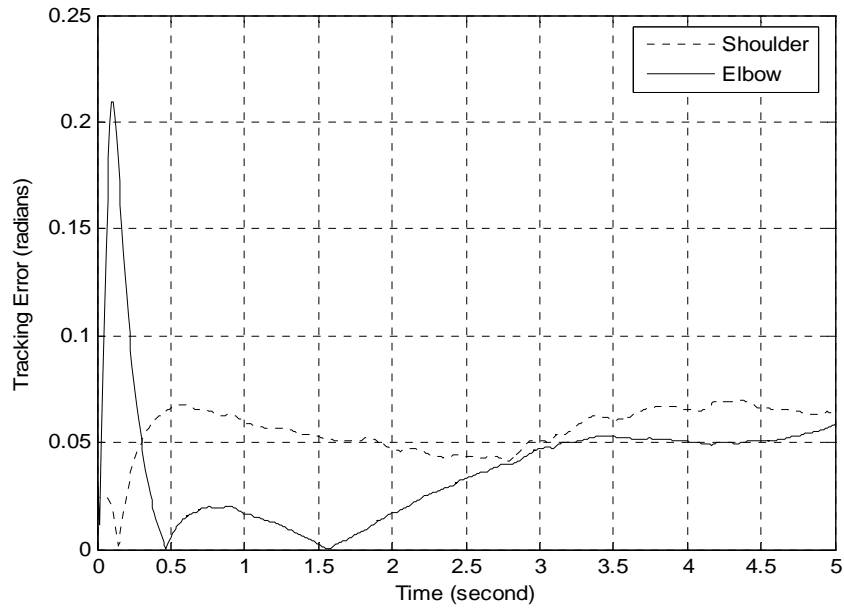
Figure 24 - Tracking errors (Spline, SMC, 10 dbw noises).

After initial transients, the tracking error of shoulder joint angle in ISMC remains within 0.01 radian and tracking error of elbow joint angle remains within 0.03 radian, while SMC errors are as large as 0.06 radian for the elbow joint and 0.07 radian for the shoulder joint.
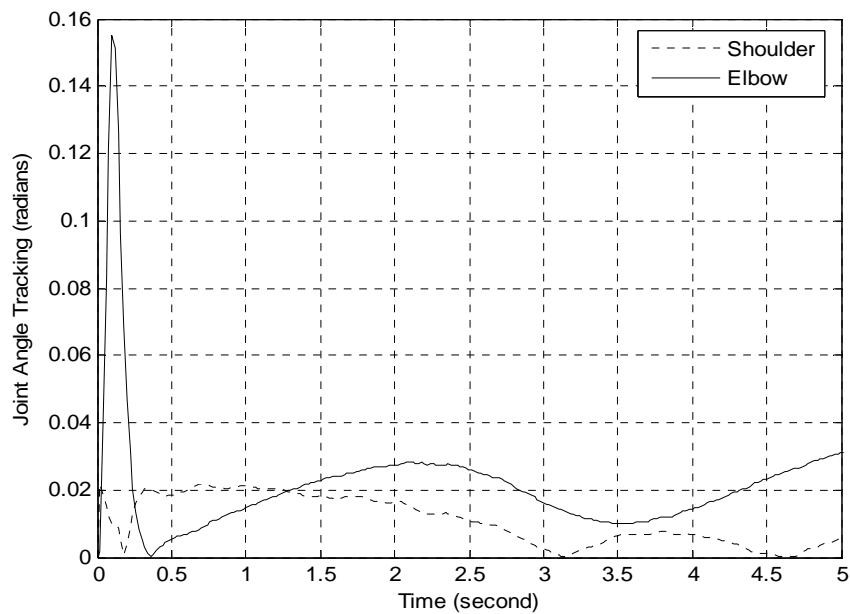

Figure 25 - Tracking errors (Spline, ISMC, 10dbw noise).
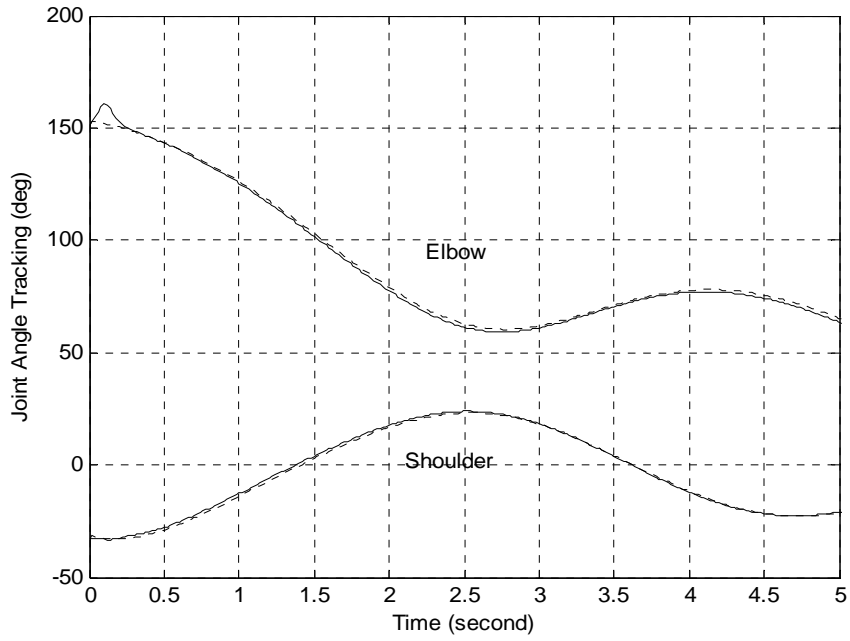
Figure 26 - Tracking performance (Spline, ISMC, 10dbw noise).
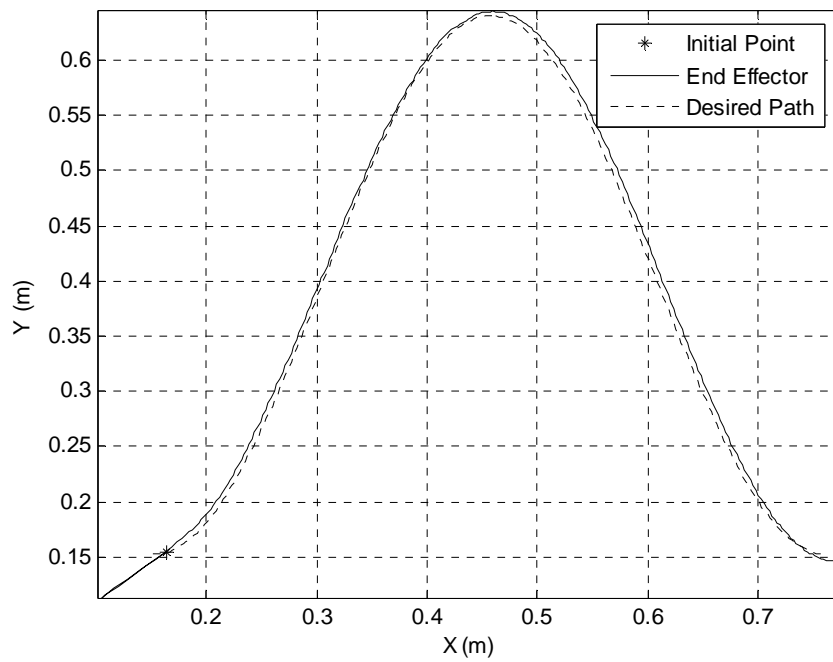

Figure 27 - Tracking path with arm (Spline, ISMC, 10dbw noise).

Figure 27 shows the end effector spatial tracking path with ISMC. From the initial point, the end effector makes some adjustments to approach the desired trajectory and tracks it very accurately afterwards. In addition, there is no obvious

chattering found from tracking trajectory generated by ISMC.

Sloping straight line:

Next, a sloping line as desired spatial path for the end effector is considered. The x and y trajectories are given by:

$$x_d(t) = 0.36576 + 0.3048\sin(0.4\pi t - 0.7754)$$
$$y_d(t) = 0.39576 + 0.3048\sin(0.4\pi t + 2.3462)$$

(8.25)

Most parameters are kept the same except that the initial conditions are set as $\theta_1(0) = 25°$, $\theta_2(0) = 100°$.
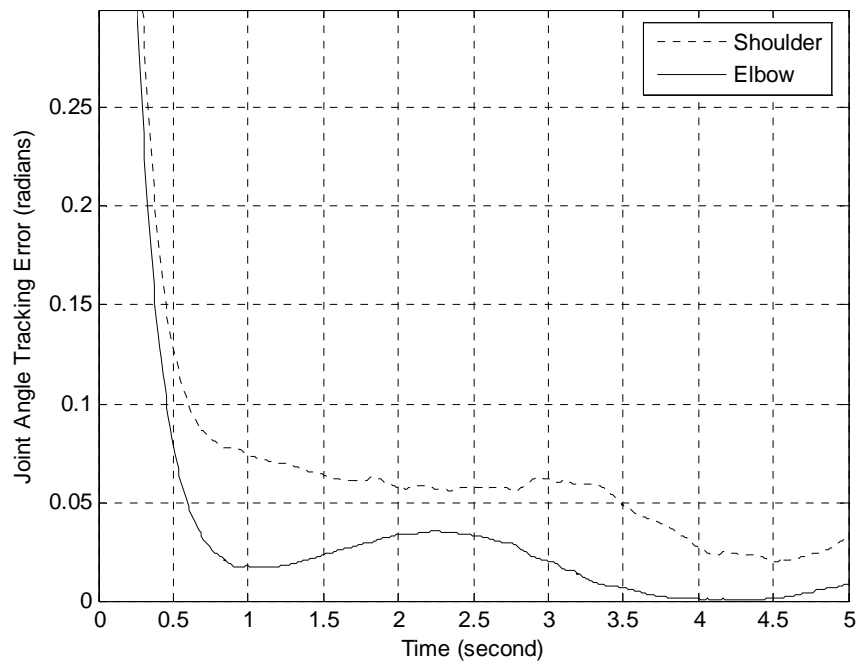

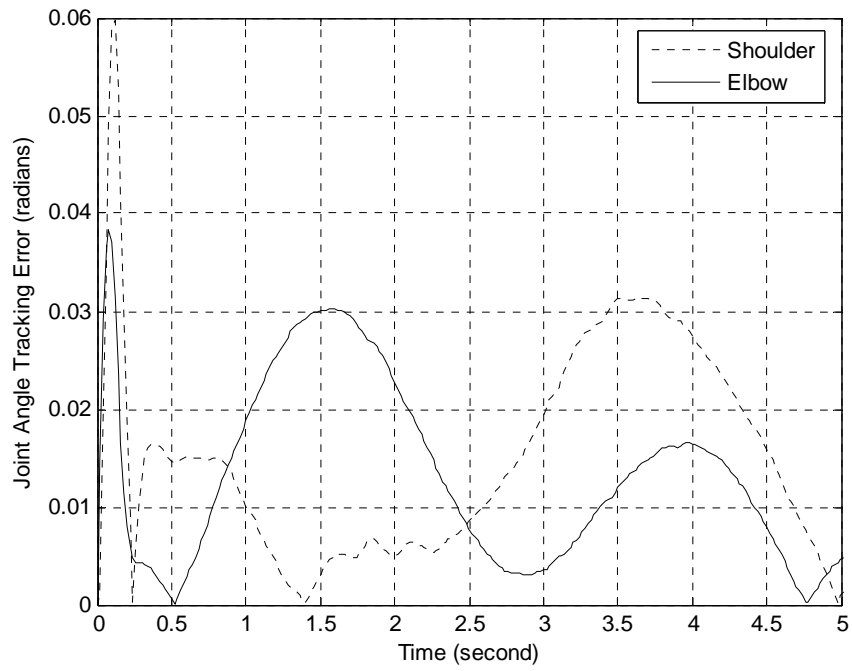Figure 28 - Tracking errors (sloping line, SMC, 10dbw noise)

Figure 29 - Tracking errors (sloping line, ISMC, 10dbw noise).
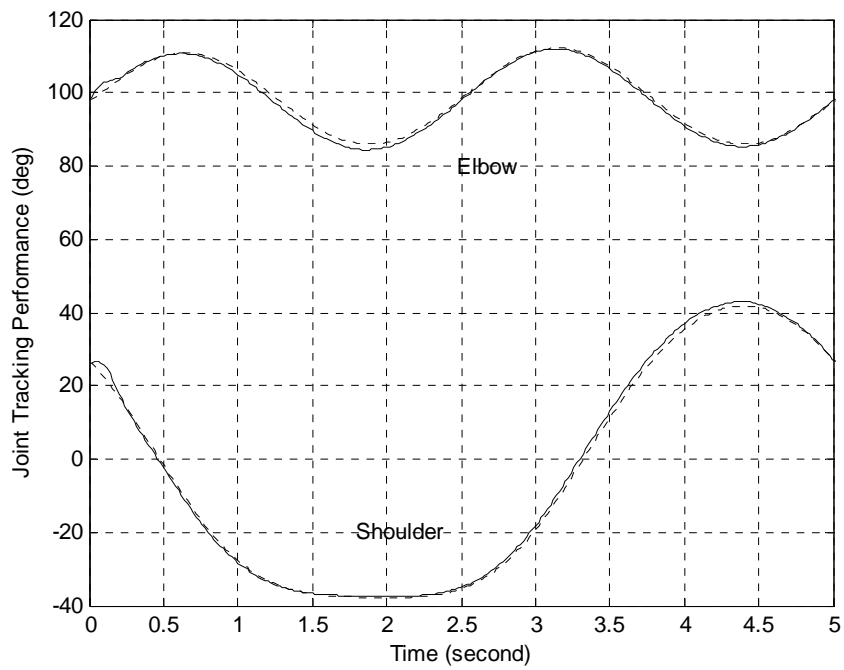
Figure 30 - Tracking performance (sloping line, ISMC, 10dbw noise).
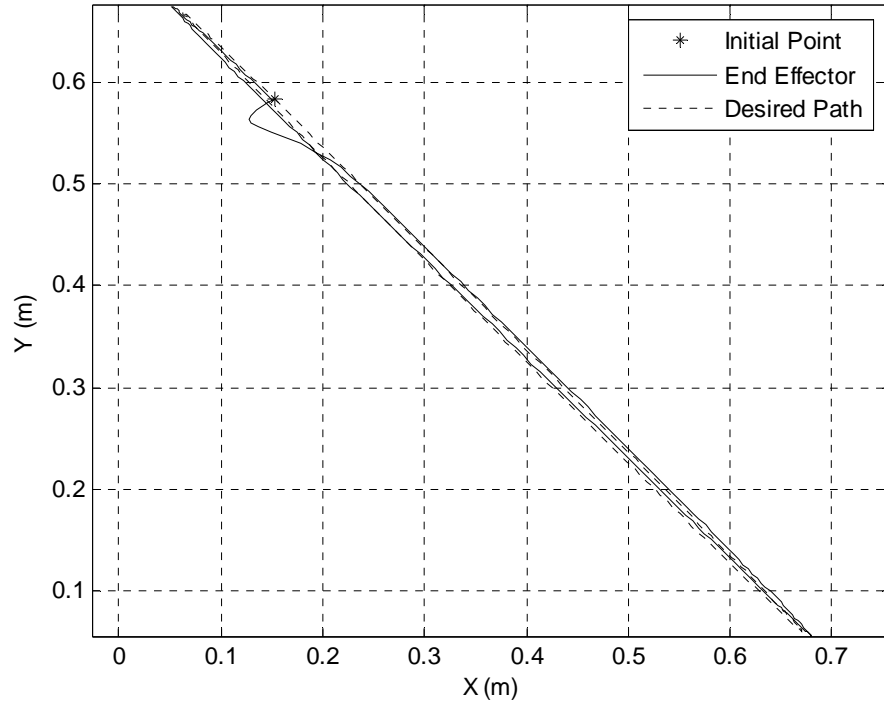
Figure 31 - Tracking path with arm (sloping line, ISMC, 10dbw noise).

Again, Gaussian white noise of 10 dbw intensity is specified. The equivalent joint angle tracking errors with SMC are shown in Figure 28 and the results from integral sliding mode control are shown in Figures 29, 30, and 31. Obviously, the better tracking performance is achieved by the proposed ISMC.

Circle:

Finally, a circle is considered as the desired spatial path for the end effector. The x and y trajectories are given by:

$$x_d = 0.36576 + 0.3048\sin(0.4\pi\,t - 0.7754)$$
$$y_d = 0.39576 + 0.3048\cos(0.4\pi\,t + 2.3462)$$

(8.26)

The simulation parameters remain the same as the first two cases. The joint angle tracking errors with SMC are shown in Figure 32 and the results from integral sliding mode control are shown in Figures 33, 34, and 35. The proposed ISMC again shows

84

better tracking performance than SMC with no chattering.
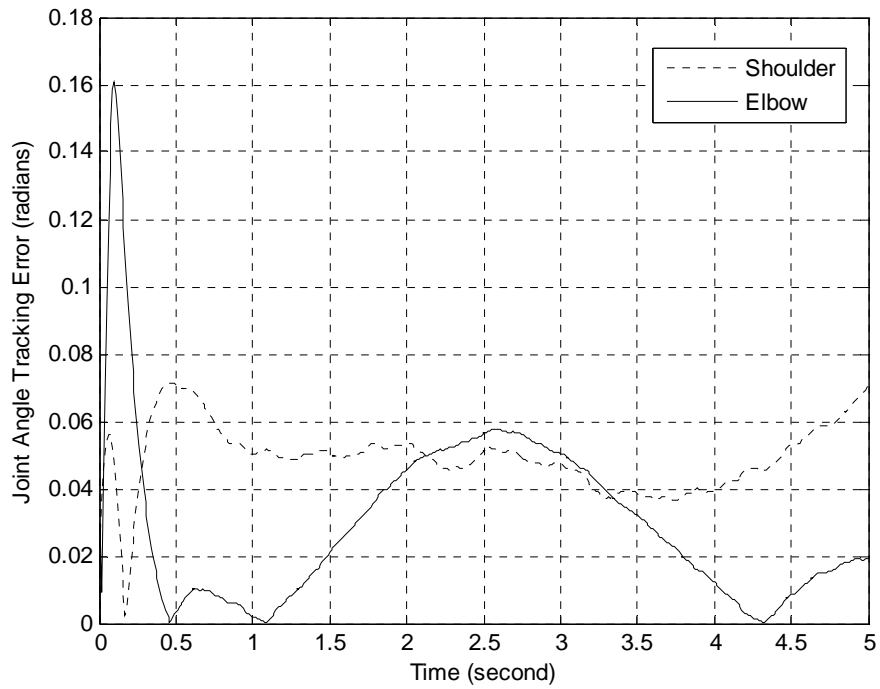
Figure 32 - Tracking errors (Circle, SMC, 10dbw noise).
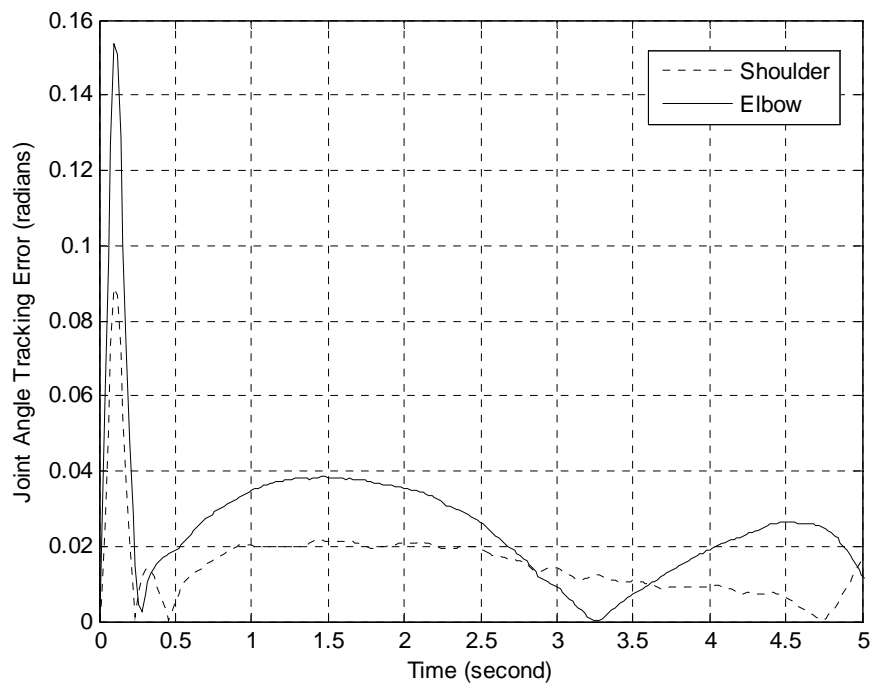
Figure 33 - Tracking errors (Circle, ISMC, 10dbw noise).
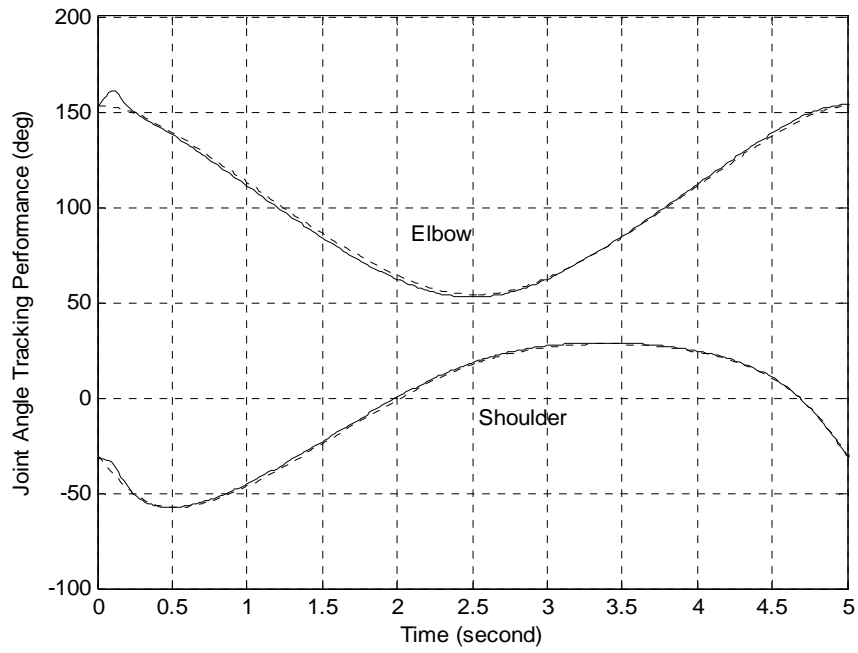
Figure 34 - Tracking performance (Circle, ISMC, 10dbw noise)
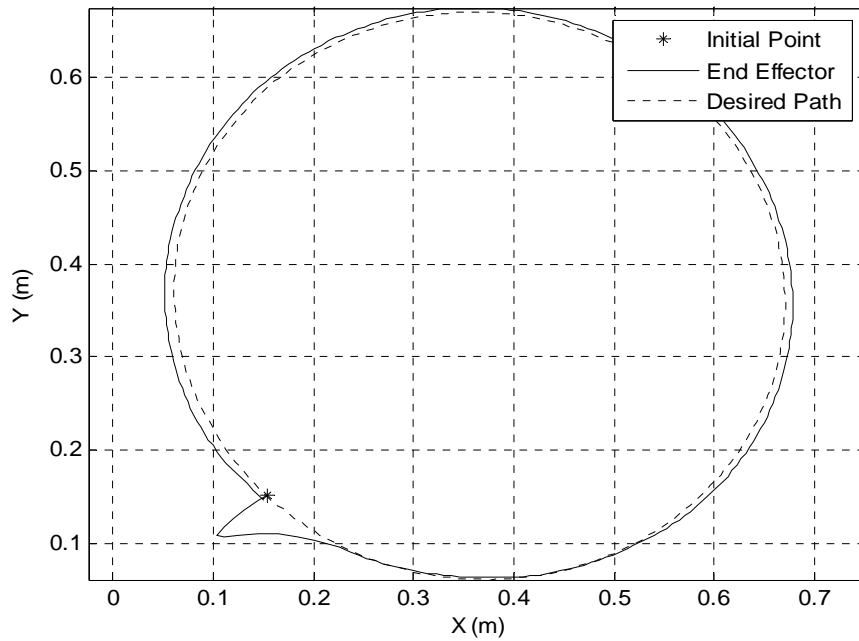
Figure 35 - Tracking path with arm (Circle, ISMC, 10dbw noise)

To study further, the intensity level of Gaussian white noise is increased to 30 dbw.   The simulation results are given in Figures 36 and 37.   From these figures it is seen that the tracking error of shoulder joint angle in ISMC is kept within 0.03

radians, while that in SMC is between 0 and 0.08 radians.   Moreover, the tracking

error of elbow joint angle in ISMC is kept within 0.04 radians while that in SMC are

between zero and 0.06 radians.   The tracking results of ISMC are obviously more

accurate than SMC.
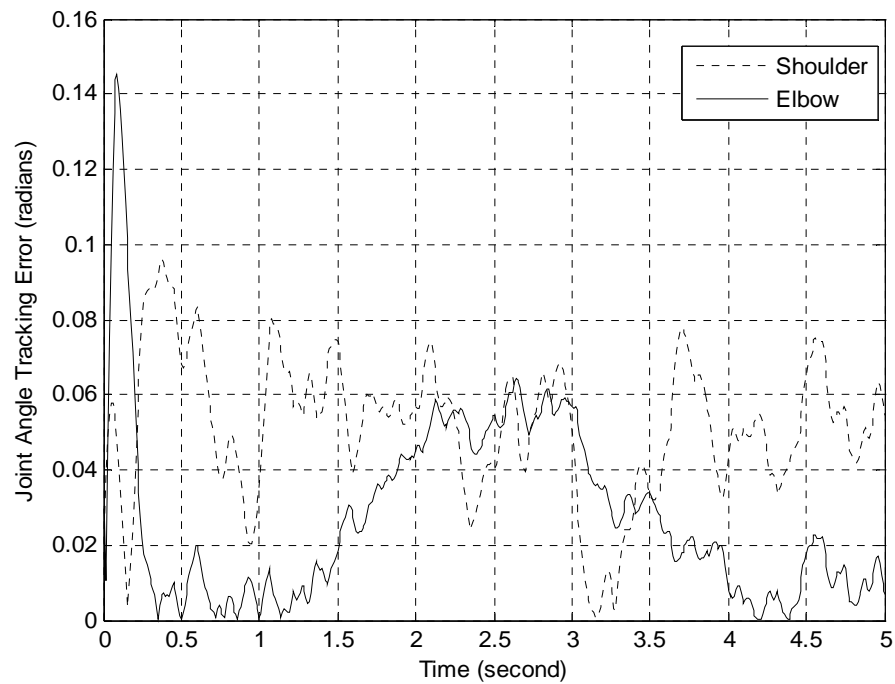
Figure 36 - Tracking error (Circle, SMC, 30dbw noise)
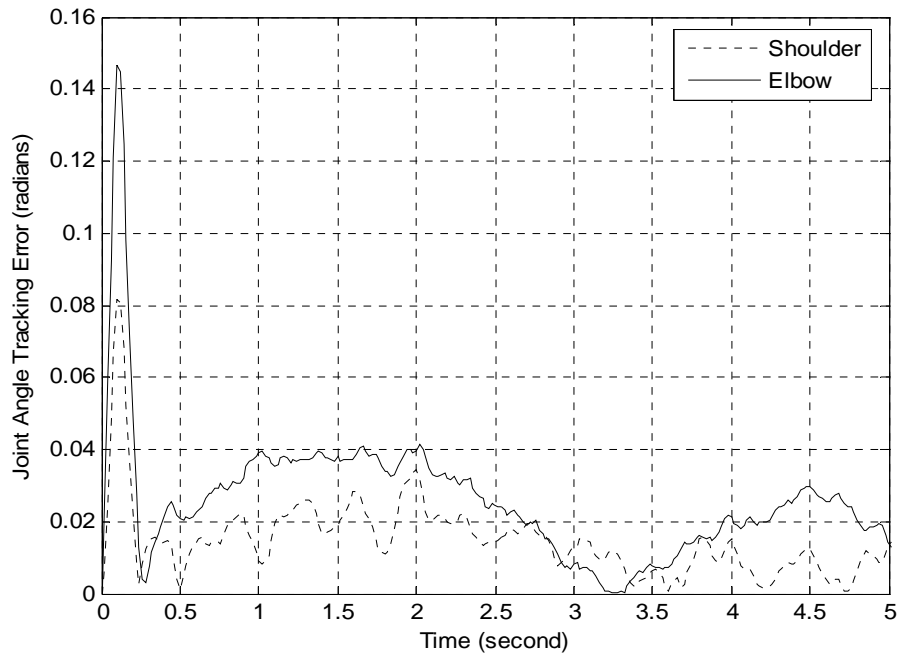
Figure 37 - Tracking error (Circle, ISMC, 30dbw noise)

To investigate the robustness of the ISMC, the intensity level of Gaussian white noise is raised to 50 dbw once again. The tracking errors for shoulder and elbow joint angle using SMC are shown in Figure 38, and those with ISMC are shown in Figure 39. The proposed ISMC retains its insensitivity without obvious change of the tracking error; however, the tracking errors from SMC are too large, hence it fails to track.

From these figures, in the presence of both modeling uncertainties and external perturbations, the control performance of the proposed ISMC is verified to be superior to SMC without obvious chattering occurring.
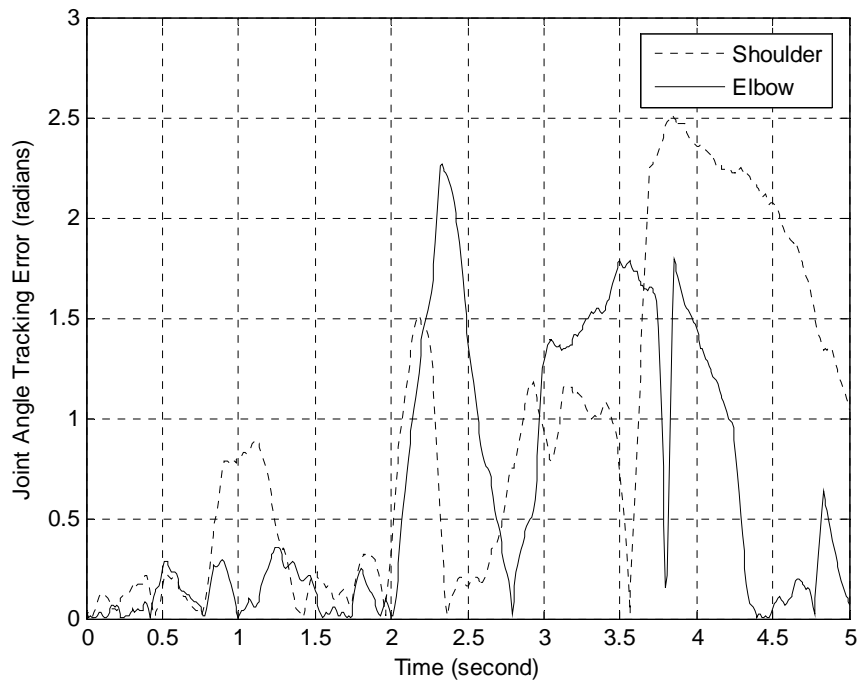
Figure 38 - Tracking error (Circle, SMC, 50 dbw noise)
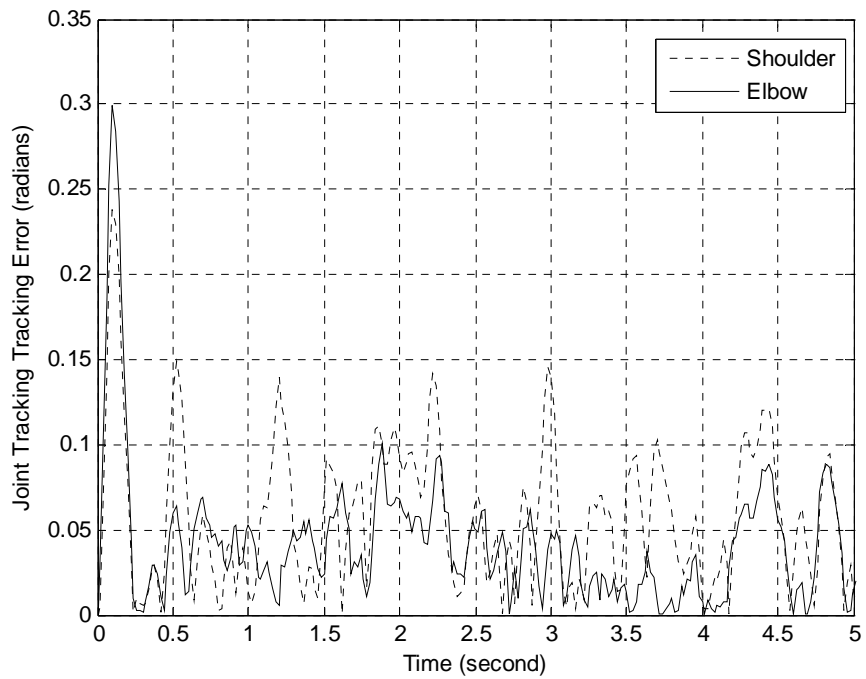
Figure 39 - Tracking error (Circle, ISMC, 50 dbw noise)

8.3 DISCUSSION

Sliding mode control (SMC) is a powerful robust control method and has been

shown as an approach with great potential to the control of PMs and robot manipulators. The "chattering" phenomenon, which is a drawback for applications of SMC, is usually reduced by introducing a boundary layer around the sliding surface.

ISMC is shown to be capable of accomplishing all the tracking tasks very well, presenting excellent tracking performance even in noisy environments. Not only in those cases does ISMC do well while traditional SMC fails, but in all circumstances, the proposed ISMC shows more precise control accuracy superior to traditional SMC. In summary, ISMC has been seen to overwhelmingly excel traditional SMC on the basis of computer simulations. Therefore it is recommended as a very promising robust control approach for tracking control of robot manipulators actuated by PMs.

CHAPTER IX
CONCLUSIONS AND CONTRIBUTIONS

9.1 CONCLUSIONS

This dissertation is concerned with development of mathematical models and control methods investigation about a certain type of planar manipulator actuated by pneumatic muscles (PMs). PMs is a novel type of actuator that closely mimics human skeletal muscles in size and power capabilities, which is considered for use in exoskeletons to be worn by humans for strength augmentation and for use as actuators in robotic systems. Since PMs are nonlinear and time-varying, perfect knowledge of PM characteristics is impossible. Moreover, the inertial parameters of robot manipulators, which depend on the payload, are often unknown and changing. Therefore, precise dynamical models of robot manipulators actuated by PMs are usually unavailable.

Sliding mode is a well-known robust control approach due to its strong insensitivity to system parameters variation. The discontinuous switching control strategy of sliding mode is designed such that a constringency property dominates the closed-loop dynamics of the nonlinear system. In this way, it induces a stabilization on the sliding surface hence the desired tracking trajectories are obtained.

In this dissertation, a one-joint and two-joint planar robot manipulators actuated by PMs are mathematically modeled. The dynamic models of the assemblies with PMs are highly nonlinear, with the control input entering the process through the nonlinear spring and friction coefficients, as well as through a nonlinear

contractile force term.   To achieve good control performance in presence of system uncertainties and external perturbation, several sliding mode control approaches have been investigated.

The design of standard sliding mode control including its stability analysis and simulations has been carried out for the one-joint planar robot manipulator model. To avoid chattering, a boundary layer is introduced around the sliding surface. Closed-loop stability is proven for the one-joint manipulator model with uncertainties, as well as a bound on the steady-state tracking error and a bound on the control effort when inside the boundary layer.

In order to reduce the steady state error while maintaining the advantageous features of traditional sliding mode controller, a two-input fuzzy sliding-mode controller has been designed for the two-joint planar arm model.   The control bandwidth is adjusted via fuzzy logic based on system tracking error.   The resulting varying sliding surface makes the tracking accuracy of fuzzy sliding mode controller better than traditional sliding mode control.   The traditional sliding mode controller and fuzzy sliding mode controller proposed show good performance on the control of the model for a robot manipulator actuated by PMs.   It needs to be pointed out that varying parameters and load variation are considered as major uncertainties in these two models.

In practice, since working environments without any noise are unavailable, some external perturbation could exist in control systems.   Therefore, a term describing the behavior of external perturbation is included in the model.   Based on the improved two-joint planar arm model, in which both system uncertainties and external disturbances are being considered now, an integral sliding mode control method is proposed.   The controller is designed with an integral sliding surface,

which plays an important role in the robust control of PM-actuated robot manipulators in face of both inner and outer uncertainties. System analysis and computer simulations are both investigated to verify that the proposed integral sliding mode control is a very promising robust control approach to handle robot manipulators actuated by PMs with parameter uncertainties and external perturbation.

9.2 CONTRIBUTIONS

The PM under investigation in this paper is one specific type, which has been developed in the Human Sensory Feedback Laboratory, Wright-Patterson Air Force Base, Dayton, Ohio. Around this PM, research relevant to system modeling and control design has been carried out. The main contribution of this dissertation is, by taking advantage of the feature of sliding mode control, along with other control methods, two effective nonlinear robust control approaches, i.e. fuzzy sliding mode control and integral sliding mode control are proposed to deal with the control of nonlinear systems containing PMs. These control approaches are validated via simulation and, where possible, theoretically. Successful applications are implemented in the tracking and motion control of PM systems through computer simulations. The principles of the analysis and control design illustrated in this paper are applicable for those systems in which other types of PMs exist, even though other PMs may result in a different model than the one used here. Another contribution is a theoretical investigation of the stability of a PM system using closed-loop state feedback control. Last but not least, the effect of heat on PM systems is addressed, and the impact on system parameters brought by the heat generated is analyzed via computer simulation.

REFERENCES

[1]   Caldwell, D.G., Medrano-Cerda, G.A., Goodwin, M., Characteristics and adaptive   control of pneumatic muscle actuators for a robotic elbow, *Proc. IEEE International Conference on Robotics and Automation*, vol.4, May 1994, 3558 – 3563.

[2]   R.T. Pack, J. L. Christopher, Jr., and Kawamura, K., A rubbertuator-based structure-climbing inspection robot,   *Proc. IEEE Int. Conf. Robotics and Automation*, Apr. 1997, 1869–1874.

[3]   Bishay, M., Cambron, M.E., Negishi, K., Peters II, R. A., and Kawamura,K., Visual servoing in ISAC, a decentralized robot system for feeding the disabled, *Proc. IEEE Int. Symp, Computer Vision*, Nov. 1995, 335–340.

[4]   Davis, S., Canderle, J., Artrit, P., Tsagarakis, N., Caldwell, D.G.., Enhanced dynamic performance in pneumatic muscle actuators, *Proc. IEEE International Conference on Robotics and Automation*, vol.3, May 2002, 2836 – 2841.

[5]   Caldwell, D.G., Medrano-Cerda, G.A., and Goodwin, M., Control of pneumatic muscle actuators," *IEEE Control Syst. Mag.*, Feb. 1995, 40–48.

[6]   Caldwell, D.G., Medrano-Cerda, G.A., and Goodwin, M. J., Braided pneumatic muscle actuators of multi-jointed manipulator, *Proc. IEEE International Conference on Systems, Man and Cybernetics*, vol.1, Oct. 1993, 423 – 428.

[7]   Tsagarakis, N., Caldwell, D.G., Improved modeling and assessment of pneumatic muscle actuators, *Proc. IEEE International Conference on Robotics and Automation*, vol.4, April 2000, 3641 – 3646.

[8]   Sanchez, A., Mahout, V., Tondu, B., Nonlinear parametric identification of a McKibben artificial pneumatic muscle using flatness property of the system, *Proc. IEEE International Conference on Control Applications*, vol.1 Sept. 1998 , 70 – 74.

[9]   Schulte, H. F., Jr., The characteristics of the McKibben artificial muscle, *The Application of External Power in Prosthetics and Orthotics*, Washington, DC: Nat. Acad. Sci., Nat. Res. Council, 1961.

[10]   Klute, G. J., Czerniecki, J. M., and Hannaford, B., McKibben artificial muscles: pneumatic actuators with biomechanical intelligence, *Proc. IEEE/ASME Int. Conf. Advanced Intelligent Mechatronics*, Sept. 1999, 21–226.

[11]   Klute, G. J., and Hannaford, B., Fatigue characteristics of McKibben artificial muscle actuators, *Proc. IEEE/RSJ Int. Conf. Intelligent Robots and Systems*, Oct. 1998, 1776–1781.

[12]   Koeneman, E.J., Schultz, R.S., Wolf, S.L., Herring, D.E., Koeneman, J.B.,A

pneumatic muscle hand therapy device, *Proc. 26th Annual International Conference of the Engineering in Medicine and Biology Society*, vol.1, 2004, 2711 – 2713.

[13]   Slotine, J-J.E., The robust control of robot manipulators, *Int. J. Rob.Res.*, vol. 4, no. 2, 1985, 49–64.

[14]   Noritsugu, T.; Tanaka, T., Application of rubber artificial muscle manipulator as a rehabilitation robot, *IEEE/ASME Transactions on Mechatronics,* vol.2, issue 4, Dec. 1997, 259 – 267.

[15]   Takaiwa, M., Noritsugu, T., Application of pneumatic parallel manipulator as haptic human interface, *IEEE/ASME International Conference on Advanced Intelligent Mechatronics*, Sept. 1999, 185 – 190.

[16]   Noritsugu, T., Tsuji, Y., Ito, K., Improvement of control performance of pneumatic rubber artificial muscle manipulator by using electrorheological fluid damper, *Proc. IEEE International Conference on Systems, Man, and Cybernetics*, vol.4, Oct. 1999, 788 – 793.

[17]   Ouerfelli, M., Kumar, V., Harwin, W., An inexpensive pneumatic manipulator for rehabilitation robotics, *Proc. IEEE International Conference on Robotics and Automation*, vol.1, May 1993, 636 – 641.

[18]   De Silva, C.W., Wong, K.H., Modi, V.J., Design development of a prototype multi-module manipulator, *Proc. IEEE/ASME International Conference on Advanced Intelligent Mechatronics,* vol.2, July 2003 1384 – 1389.

[19]   Berkelman, P., Cinquin, P., Troccaz, J., Ayoubi, J., Letoublon, C., Bouchard, F., A compact, compliant laparoscopic endoscope manipulator**,** *Proc. IEEE International Conference on Robotics and Automation*, vol.2, May 2002, 1870 – 1875.

[20]   Caldwell, D.G., Tsagarakis, N., Medrano-Cerda, G.A., Schofield, J., Brown, S., Development of a pneumatic muscle actuator driven manipulator rig for nuclear waste retrieval operations, *Proc. IEEE International Conference on Robotics and Automation*, vol.1, May 1999, 525 – 530.

[21]   Slotine, J-J., Li, W., *Applied Nonlinear Control*, Prentice Hall, 1991.

[22]   Paul, A.K., Mishra, J.E., Radke, M.G., Reduced order sliding mode control for pneumatic actuator**,** *IEEE Transactions on Control Systems Technology*, vol.2, issue 3, Sept. 1994, 271 – 276.

[23]   Carbonell, P., Jiang, Z.P., Repperger, D.W., Nonlinear control of a pneumatic muscle actuator: backstepping vs. sliding-mode, *Proc. IEEE International Conference on Control Applications*, Sept. 2001, 167 – 172.

[24]   Su, C.-Y., Leung, T.-P., A sliding mode controller with bound estimation for robot manipulators, *IEEE Transactions on Robotics and Automation*, vol.9, issue 2, April 1993, 208 – 214.

[25]   Van der Zalm, G., Kostic, D., De Jager, B., Discrete-time sliding mode control of a direct-drive robot manipulator, *Proc. 43rd IEEE Conference on Decision and Control*, vol.2, Dec. 2004, 1234 – 1239.

[26]   Istefanopulos, Y., Jafarov, E.M., Parlakci, M.N.A., A new robust continuous sliding mode control for robot manipulators with parameter perturbations, *Proc. American Control Conference*, vol.4, May 2002, 3202 – 3206.

[27]   Mozaryn, J., Kurek, J.E., Design of decoupled sliding mode control for the PUMA 560 robot manipulator, *Proc. the Third International Workshop on Robot Motion and Control*, Nov. 2002, 45 – 50.

[28]   Istefanopulos, Y., Jafarov, E.M., Parlakci, M.N.A., A new robust continuous sliding mode control for robot manipulators with parameter perturbations, *Proc. American Control Conference*, vol.4, May 2002, 3202 – 3206.

[29]   Yang, D., Yamane,Y., Zhang,X., Zhu, R., A sliding mode control of robot manipulator with variable payload, *Proc. IEEE International Conference on Intelligent Processing Systems*, vol.2, Oct. 1997, 1312 – 1316.

[30]   Yi, S., Chung, M., A robust fuzzy logic controller for robot manipulators with uncertainties, *IEEE Transactions on Systems, Man and Cybernetics*, vol.27, issue 4, Aug. 1997, 706 – 713.

[31]   Santibanez,V., Kelly, R., Llama, M.A., Global asymptotic stability of a tracking sectorial fuzzy controller for robot manipulators, *IEEE Transactions on Systems, Man and Cybernetics*, vol.34, issue 1, Feb. 2004, 710 – 718.

[32]   Ham, C., Qu, Z., Johnson, R., Robust fuzzy control for robot manipulators, *Proc. Control Theory and Applications*, vol.147, issue 2, March 2000 212 – 216.

[33]   Bekit, B.W., Whidborne, J.F., Seneviratne, L.D., Fuzzy sliding mode control for a robot manipulator, *Proc. IEEE International Symposium on Computational Intelligence Robotics and Automation*, July 1997, 320 – 325.

[34]   Kwok, N., Lee, C., Control of a flexible manipulator using a sliding mode controller with a fuzzy-like weighting factor, *Proc. IEEE International Symposium on Industrial Electronics*, vol.1, June 2001, 52 – 57.

[35]   Ahmad, M.N., Osman, J.H.S., Robust sliding mode control for robot manipulator tracking problem using a proportional-integral switching surface, *Proc. Student Conference on Research and Development*, Aug. 2003, 29 – 35.

[36]   Ahmad, M.N., Osman, J.H.S., Application of Proportional-Integral sliding mode tracking controller to robot manipulators, *Proc. IEEE Conference on Control Applications*, vol.1, June 2003, 87 – 92.

[37]   Noh Ahmad, M., Osman, J.H.S., Ruddin A.,Ghani, M., Decentralized proportional-integral sliding mode tracking controller for robot manipulators, *Proc. IEEE Conference on Computers, Communications, Control and Power Engineering* ,

vol.3, Oct. 2002, 1314 – 1317.

[38]   Xu, J., Pan,Y., Lee,T., Analysis and design of integral sliding mode control based on Lyapunov's direct method, *Proc. American Control Conference*, vol.1, June 2003, 192 – 196.

[39]   Utkin, V., Shi, J., Integral sliding mode in systems operating under uncertainty conditions , *Proc. 35th IEEE Conference on Decision and Control*, vol.4, Dec. 1996, 4591 – 4596.

[40]   Zhuang, K., Su, H., Chu, J., Zhang, K., Globally stable robust tracking of uncertain systems via fuzzy integral sliding mode control, *Proc. 3rd World Congress on Intelligent Control and Automation*, vol.3, July 2000, 1827 – 1831.

[41]   Reynolds, D.B., Repperger, D.W, Philips, C.A., and Bandry, G., Modeling the Dynamic Characteristics of Pneumatic Muscle, *Annals of Medical Biomedical Engineering*, Mar. 2003, 310-317.

[42]   Utkin, V.I., *Sliding modes in control and optimization*, Springer-Verlag, 1992.

[43]   Bowler, C.J, Caldwell, D.G, Medrano-Cerda, G.A, Pneumatic muscle actuators: musculature for an anthropomorphic robot arm, *Proc. IEE Colloquium on Actuator Technology*, May 1996, 8/1 – 8/6.

[44]   Lilly, J.H., Adaptive tracking for pneumatic muscle actuators in bicep and tricep configurations, *IEEE Transactions on Neural Systems and Rehabilitation Engineering*, vol.11, issue.3, Sept. 2003, 333 – 339.

[45]   Caldwell, D.G, Tsagarakis, N, Badihi, D, Medrano-Cerda, G.A, pneumatic muscle actuator technology: a light weight power system for a humanoid robot, *Proc. Robotics and Automation*, vol.4, May 1998, 3053 – 3058.

[46]   Yang, L., Lilly, J.H., Sliding mode tracking for pneumatic muscle actuators in bicep/tricep pair configuration, *Proc. American Control Conference*, vol.6, June 2003, 4669 – 4674.

[47]   Balasubramanian, K., Rattan, K.S., Feedforward control of a non-linear pneumatic muscle system using fuzzy logic, *Proc. 12th IEEE International Conference on Fuzzy Systems*, vol.1, May 2003, 272- 277.

[48]   Chan, S.W, Lilly, J.H., Repperger, D.W., Berlin, J.E., Fuzzy PD+I learning control for a pneumatic muscle, *Proc. 12th IEEE International Conference on Fuzzy Systems*, vol.1, May 2003, 278 – 283.

[49]   Park, C., Kim, J., Kwon,C., Park,M., Tracking control of a robot manipulator using sliding mode controller with fast and accurate performance, *Proc. 1999 international conference on intelligent robots and systems*, vol.1, Oct. 1999, 305-310.

[50]   Djouadi, S.M., Repperger, D.W., Berlin, J.E., Gain-scheduling H^∞ control of a pneumatic muscle using wireless MEMS sensors, *Proc. 44th IEEE 2001 Midwest Symposium on Circuits and Systems*, vol.2, August, 2001,734 – 737.

[51]   Repperger, D.W., Johnson, K.R., Phillips, C.A., A VSC position tracking system involving a large scale pneumatic muscle actuator, *Proc. 37th IEEE Conference on Decision and control,* vol.4, Dec. 1998, 4302 – 4307.

[52]   Medrano-Cerda, G.A., Bowler, C.J., Caldwell, D.G., Adaptive position control of antagonistic pneumatic muscle actuators, *Proc. IEEE/RSJ International Conference on Intelligent Robots and System*, vol.1, August 1995, 378 – 383.

[53]   Zeller, M., Sharma, R., Schulten, K., Motion planning of a pneumatic robot using a neural network, *IEEE Control Systems Magazine*, vol.17, issue.3, June 1997, 89 – 98.

[54]   Hamdan, M., Gao, Z., A novel PID controller for pneumatic proportional valves with hysteresis, *Proc. Industry Applications Conference*, vol.2, Oct. 2000, 1198 – 1201.

[55]   Balasubramanian, K., Rattan, K.S., Fuzzy logic control of a pneumatic muscle system using a linearizing control scheme, *North American Fuzzy Information Processing Society*, July 2003, 432 – 436.

[56]   Parnichkun, M., Ngaecharoenkul, C., Hybrid of fuzzy and PID in kinematics control of a pneumatic system, *Industrial Electronics Society*, vol.2, Oct.2000, 1485 – 1490.

[57]   Lilly, J.H., Quesada, P.M., A two-input sliding mode controller for a planar arm actuated by four pneumatic muscle groups, *IEEE Transactions on Neural Systems and Rehabilitation Engineering*   vol.12, issue.3, Sept. 2004,349 – 359.

[58]   Lewis, F.L., Abdallah, C.T., Dawson, D.M., *Control of Robot Manipulators*, Macmillan Publishing, Company, 1993.

[59]   Perruquetti, W., Barbot, J.P., *Sliding Mode Control in Engineering*, Marcel Dekker, Inc., 2002.

[60]   Utkin, V, Variable structure systems with sliding modes, *IEEE Transactions on Automatic Control*, vol.22, issue 2, Apr 1977, 212 – 222.

[61]   Wang, J., Lee,T., Juang,Y., New methods to design an integral variable structure controller, *IEEE Transactions on Automatic Control*,vol.41 , issue 1, Jan.1996, 140 – 143.

[62]   Rios-Gastelum, O.G.., Castillo-Toledo, B., Loukianov, A.G., nonlinear block integral sliding mode control: application to induction motor control, *Proc. 42nd IEEE Conference on Decision and Control*, vol.3, Dec. 2003, 3124 – 3129.

[63]   Lee, J., Youn, M., A new integral variable structure regulation controller for

robot manipulators with accurately predetermined output, *Proc. IEEE International Symposium on Industrial Electronics*, vol.1,12-16 July 1999, 336 – 341.

[64]   Lilly, J. H., Yang, L., Sliding mode tracking for pneumatic muscle actuators in opposing pair configuration, *IEEE Transactions on Control Systems Technology*, Vol.13, No.4, pp.550-558, July 2005.

[65]   Comer, Alan Elbert, Pneumatic muscle analogs for exoskeletal robotic limbs and associated control mechanisms, *Unite States Patent*, 5,014,600, Feb. 2004.

[66]   Krauter, Allen I., et, al, Bistep terminator for hydraulic or pneumatic muscle, *Unite States Patent*, 6,684,754, May, 1991.

[67]   Minami, Mamoru, Method of controlling position and attitude of working robot and its manipulator and apparatus thereof, *Unite States Patent*, 5,542,028, July, 1996.

[68]   Gamble, Jonathan, Sliding model control system, *Unite States Patent*, 5,285,379, Feb. 1994.

[69]   Schlemmer, Maximilian, Method of command control for a robot manipulator, *Unite States Patent*, 6,181,983, Jan. 2001.

[70]   Yoneda, Koji, Motion controller having sliding mode controller, *Unite States Patent*, 4,019,482, Mar. 2006.

CURRICULUM VITAE

NAME:　　　　Liang Yang

ADDRESS:　　　Department of Electrical and Computer Engineering
　　　　　　　　University of Louisville
　　　　　　　　Louisville, KY 40292

DOB:　　　　　Chongqing, China – September 5, 1975

EDUCATION:

　　　　　　　　B.S., Electrical Engineering
　　　　　　　　Sichuan University, China
　　　　　　　　1994-1998

　　　　　　　　M.S., Electronic Engineering
　　　　　　　　Sichuan University, China
　　　　　　　　1998-2001

　　　　　　　　PhD, Electrical Engineering
　　　　　　　　University of Louisville, KY
　　　　　　　　2001-2006

TEACHING:

　　　　　　　　Teaching Assistant,
　　　　　　　　Department of Electrical and Computer Engineering
　　　　　　　　University of Louisville

　　　　　　　　Taught labs for courses as follows:
　　　　　　　　ECE 334 "Electronics".

ECE 422 "Active Network Design".

ECE 536 "Instrumentation Electronics".

RESEARCH SUPPORT:

Air Force Office of Scientific Research Grant "Pneumatic Muscle Actuator Control".

PROFESSIONAL SOCIETIES:

Eta Kappa Nu (National ECE Honor Society).

FE Certification

PUBLICATIONS:

Liang Yang**,** J.H. Lilly, Sliding mode tracking for pneumatic muscle actuators in bicep/tricep pair configuration, *Proc. American Control Conference*, Vol.6, pp.4669 – 4674, June 2003.

J.H. Lilly**,** Liang Yang, Sliding mode tracking for pneumatic muscle actuators in opposing pair configuration, *IEEE Transactions on Control Systems Technology,* Vol.13, No.4, pp.550-558, July 2005.

Liang Yang, J.H. Lilly**,** A fuzzy sliding mode controller for a two-joint manipulator actuated by pneumatic muscles, *Intelligent Automation and Soft Computing,* under revision.

Liang Yang, J.H. Lilly**,** An integral sliding mode approach for tracking control of a planar robot arm actuated by pneumatic muscles, pending to submission.